CubeSat On-Orbit Temperature Comparison to Thermal-Balance-Tuned Model Predictions

James Paul Mason[a] and Bret Lamprecht[b] and Thomas N. Woods[c]
University of Colorado, Boulder, CO, 80303, USA

Chloe Downs[d]
University of Virginia, Charlottesville, VA, 22904-4714, USA

Confidence in spacecraft thermal models can be built by tuning their numerous parameters using the results of a thermal balance test. In such a test, the flight article is placed in a thermal vacuum chamber configured to be as similar to the orbital environment as possible. High power-draw subsystems in the spacecraft are "pulsed" on for a few minutes so that the heat propagation through the system can be measured and conductive values in the model tuned. The thermal model can then be used to make more reliable predictions for the orbital temperatures. The ultimate validation of the model is comparison of the predictions to the actual on orbit measured temperatures. This paper describes the procedure, analysis, and results of all of the above as they apply to the first Miniature X-ray Solar Spectrometer (MinXSS-1) 3U CubeSat. MinXSS-1 was deployed from the International Space Station on 2016 May 16 and deorbited on 2017 May 06. Many of the tuned-model parameters are applicable to other CubeSats and could provide a baseline for programs that do not have the resources to dedicate to detailed thermal modeling and testing. We find generally good agreement, to within a few °C, between the thermal model and the actual orbital measurements.

[a] Research Scientist, Laboratory for Atmospheric and Space Physics
[b] Professional Research Assistant, Laboratory for Atmospheric and Space Physics
[c] Senior Research Scientist, Laboratory for Atmospheric and Space Physics, AIAA Senior Member
[d] Student, Physics, University of Virginia

I. Introduction

The purpose of thermal modeling for a spacecraft is to ensure that all components will stay within their operational and survival temperature limits while on orbit. That includes the science instruments, which frequently require very low temperatures and thermal stability. Thus, science instruments are often the most restrictive element and as such can drive the thermal design. This was the case for the Miniature X-ray Solar Spectrometer (MinXSS) 3U CubeSat, whose primary science instrument, a modified Amptek X123 silicon drift detector soft X-ray spectrometer, must keep its detector at -50 °C. The X123 ships with an integrated thermal electric cooler (TEC) to achieve this, but its heat sink must be kept below +35 °C.

This paper first describes the satellite and testing hardware, as well as a brief introduction to the tests performed and software used in section II. Then in III, it describes the thermal vacuum balance (TVAC) and thermal balance (TBAL) testing that was performed, including tank configurations and procedures. IV describes the Thermal Desktop model in its “correlated", post-TBAL-analysis state. V shows how close the model comes to the measured TBAL values and describes some of the tuning that took place. The spacecraft thermal model is then placed into a modeled International Space Station (ISS) orbit and temperature predictions produced to be compared to the actual on-orbit measurements in VI. The last section, VII, summarizes the results and draws conclusions. The appendices provide the Thermal Desktop model parameters.

II. Program Description

MinXSS-1 is the first of two nearly identical CubeSats and was launched on 2015 December 6 to the International Space Station. It was deployed from the airlock on 2016 May 16. MinXSS-1 was been stably Sun-pointed for the entire mission until the last few hours of the mission, which ended on 2016 May 06. The X123 measures soft X-ray spectra from the Sun in the range 0.4 - 30 Å (0.4 - 30 keV) with up to 0.15 keV (0.8 Å) resolution [1, 2]. This range of the solar spectrum is expected to contain the greatest irradiance enhancement from solar flares [3], is known to have an important impact in the Earth's ionospheric E-region [4], and can be used to estimate coronal abundances and discriminate between competing coronal heating theories [5]. Further detail about the science case and overview of the system can be found in [6].

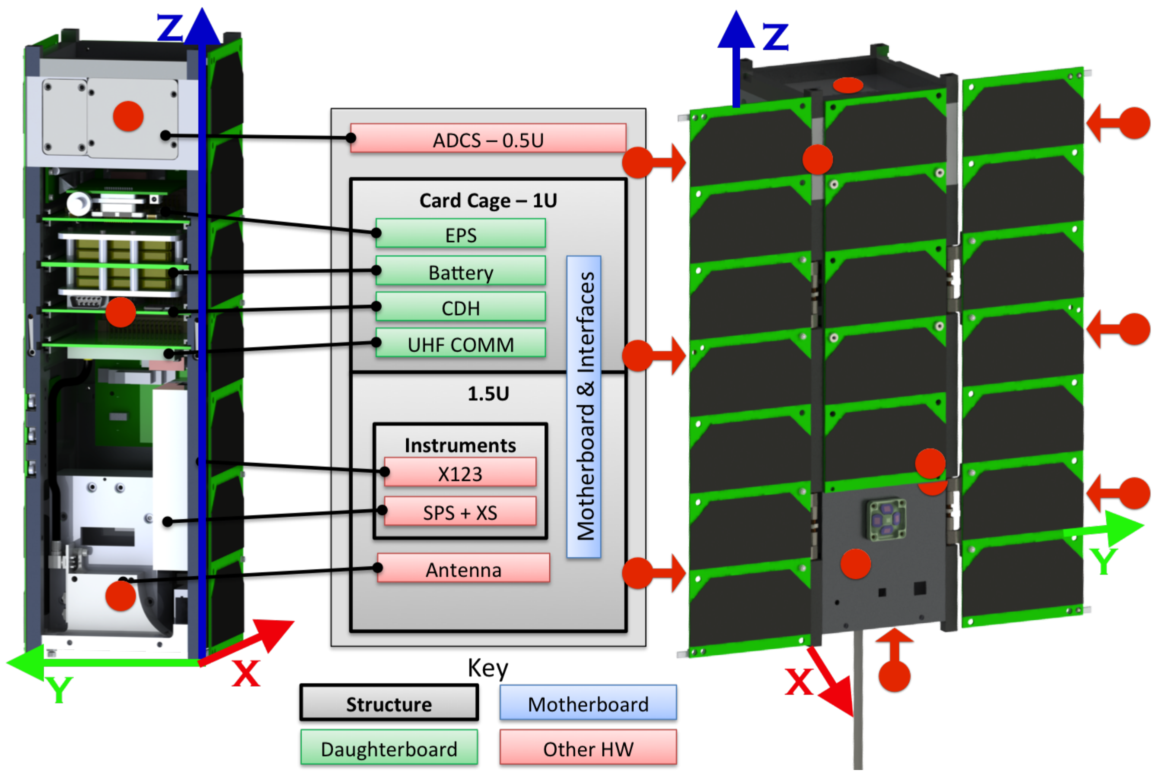

Fig. 1 MinXSS mechanical block diagram and reference coordinate system. On orbit, +X is to the Sun and +Y is nadir. The red dots indicate the approximate location of thermocouples placed on the structure for thermal balance testing. Modified and reproduced from [6]

Figure 1 shows the mechanical block diagram of MinXSS with a Cartesian coordinate system that will be referred to throughout this paper. The structure consists of 5 custom-machined Aluminum 6061 plates bolted together, with a Blue Canyon Technologies XACT attitude determination and control system (ADCS) and a 4-post bracket bolted to the +Z side. The structural bolts are all #4 size and of various lengths. Most of the outside surfaces have been covered with silver-coated Teflon tape. Inside, a motherboard runs most of the length of the CubeSat on the Sun-facing (+X) side and minimizes the number of cables needed to interface subsystems. The electrical power system (EPS) board, command and data handling (CDH) board, communications (COMM) board, and the battery board are referred to as the “daughterboards" because they plug into the motherboard (with the exception of a direct cable running between the battery and EPS boards). The science instruments – the X123 and SPS/XP – also plug into the motherboard. Each of the daughterboards is mechanically fixed with Unitrack Kooler-Guide rails on the Y sides, which clamp the boards with copper-beryllium springs to provide improved thermal conductivity out of the boards. Each daughterboard, other than the battery board, has a copper layer in the printed circuit board (PCB) for better thermal conductivity away from the heat-generating electrical components. The battery board does not contain this copper plane to intentionally thermally isolate it from the rest of the system. The X123 is directly bolted to the -Y plate and its detector head includes a dedicated thermal electric cooler. Figure 2 shows the thermal zones of the system. The implementation details of the system abound, but the CubeSat standard itself means that the MinXSS design has more similarities than differences with other CubeSats.

Several software packages exist for thermal modeling. Thermal Desktop was used for MinXSS. This software offers many advanced tools that go beyond what is necessary for most CubeSats so some teams have developed their own simpler tools (e.g., **(author?)** 7, 8). While prior studies have compared thermal model results to Thermal Desktop and on-orbit data, to the best of our knowledge, no one has published a CubeSat model comparison to dedicated thermal balance testing. Thermal balance tests use a similar configuration to thermal vacuum cycle testing but seek to create a stable thermal environment for correlating model temperatures and tuning model parameters.

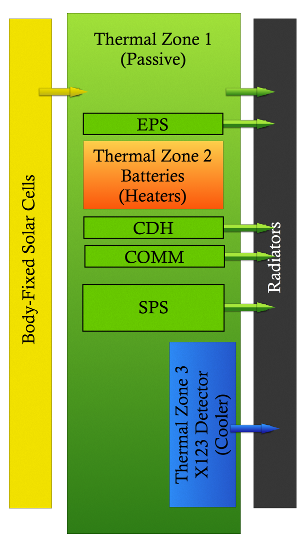

Fig. 2 MinXSS-1 thermal zone block diagram.

TVAC cycle testing consists of several hot and cold periods with the space-craft in operation

Table 1 Thermal requirements

Component	Operating Range [°C]	Survival Range [°C]
ADCS	[-20, +60]	[-20, +60]
CDH, EPS, motherboard	[-30, +70]	[-40, +85]
Li-polymer batteries	[0, +40]	[-20, +70]
Radio	[-30, +70]	...
Solar panels	[-75, +100]	[-75, +100]
X123 detector heat sink	[-20, +35]	[-60, +60]
X123 electronics	[-20, +50]	[-40, +85]

while in a vacuum environment [9]. This stresses the system in an environment that is much more flight like than bench testing. TVAC testing is not required by the Cal Poly CubeSat Design Specification (CDS, **(author?)** 10), the NanoRacks Interface Control Document (ICD, **(author?)** 11), or most launch providers. Nevertheless, it is best practice to perform this test, which is very valuable for catching mission-ending issues. Lessons learned from the MinXSS TVAC testing are summarized in III A and details can be found in [6].

TBAL testing has similar test configuration to TVAC cycling but it instead strives to reach thermal equilibrium in a hot and cold case to have a steady-state configuration to directly compare a thermal model with measurements [9]. Ideally, these will be the worst case hot and cold on-orbit environments. Additionally, heat load transients can be triggered against this background to characterize heat flow through the system. For MinXSS, the environment was made even more flight-like than during TVAC cycling: one surface of the chamber was made hot to simulate solar input and the rest of the chamber was made cold to simulate deep space. Several aspects of the analysis herein have been made as generic as possible so as to maximize the applicability to other CubeSat missions, including our own future work. The operating and survival temperatures for the major components of MinXSS are listed in Table 1, all of which are common among CubeSats, except for the science payload (the X123).

III. Test Procedures

A. TVAC Overview

The thermal vacuum chamber used for MinXSS testing was BEMCO-West at the Laboratory for Atmospheric and Space Physics (LASP). The chamber is a long cylinder with a 0.76 m diameter and 1.22 m length. Two independently controlled temperature surfaces are inside: a large flat platen along the bottom and a curved shroud around the sides and top. MinXSS was placed near the back of the chamber with its -X side facing down (Figure 3). MinXSS was clamped down to a custom aluminum U-plate that was designed to mirror the P-POD rail and empty volume dimensions. This design ensured that there would be no mechanical interference with sensitive components on the spacecraft (e.g., solar panels) if a different spacecraft orientation was to be used inside the U-plate. The U-plate was also designed to hold both MinXSS flight models end-to-end for other testing that was performed. The U-plate was bolted down with 18 1/4"-20 bolts. The goal was to maximize the thermal conduction between the chamber's platen and the spacecraft. This meant having as few mechanical interfaces as possible, as much surface area contact as possible, and a tight seal between all mechanical interfaces. Thermocouples (TCs), were adhered to each face of the spacecraft. The $\pm$ X TCs were used as the feedback for the control loop.

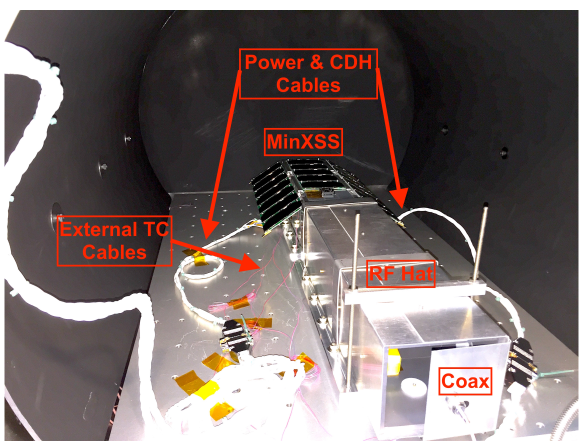

Fig. 3 MinXSS-1 in BEMCO-West TVAC chamber with labels.

A solar array simulator (SAS) was plugged into the EPS board in place of the actual solar panels and power settings were based on the measured values of the solar cells from the lot specification sheet. The SAS can generate an arbitrary solar cell power curve given three points on the I-V curve.

For MinXSS-1, these values were $I_{sc} = 1.5A$, $I_{mp} = 1.41A$, $V_{oc} = 17.5V$, and $V_{mp} = 16.4V$, where I is current, V is voltage, sc is short circuit, oc is open circuit, and mp is maximum power. The SAS can be controlled by a computer via USB; an in-house MATLAB graphical user interface (GUI) was developed to provide a means of changing the power settings, including an autonomous timer to simulate an orbit by power cycling, e.g., on for 60 minutes, off for 30 minutes, and repeat. Three orbital scenarios were simulated: average eclipse time, maximum eclipse time, and minimum eclipse time. Since MinXSS-1 was to be deployed from the ISS, we used parameters from such an orbit; they are specified in Table 2. It was not possible to also cycle the hot platen because its temperature transitions take longer than the duration of an orbit. Thus, we had to accept this limitation of the test.

Table 2 TVAC SAS orbit time settings (total orbit period in all cases is 93 min)

Configuration	Eclipse Duration [min]	Insolation Duration [min]
Average Eclipse	28	65
Maximum Eclipse	38	55
Minimum Eclipse	0	93

The procedure for TVAC cycling was typical: hot survival, cold survival, then a series of hot/cold operational cycles with dwell periods at each. For MinXSS-1, hot survival was +60 oC and cold survival was -30 oC. Hot cycle was +30 oC and cold cycle was -20 oC. Eight cycles in total were completed, with a 3 hour dwell at each point. The platen and shroud set points were more extreme than the target temperatures in order to drive the $\pm$ X TCs on MinXSS to the targets. All of the parameters of this test were less stringent than but in the same spirit as the NASA standards [9] required of larger missions, but still sufficient to convince the MinXSS team that the system would operate well on orbit. Note that these tests were not required by any external agencies but because they are a best practice, they were conducted. Figure 4 shows the planned temperature cycles and the actual X plate temperatures.

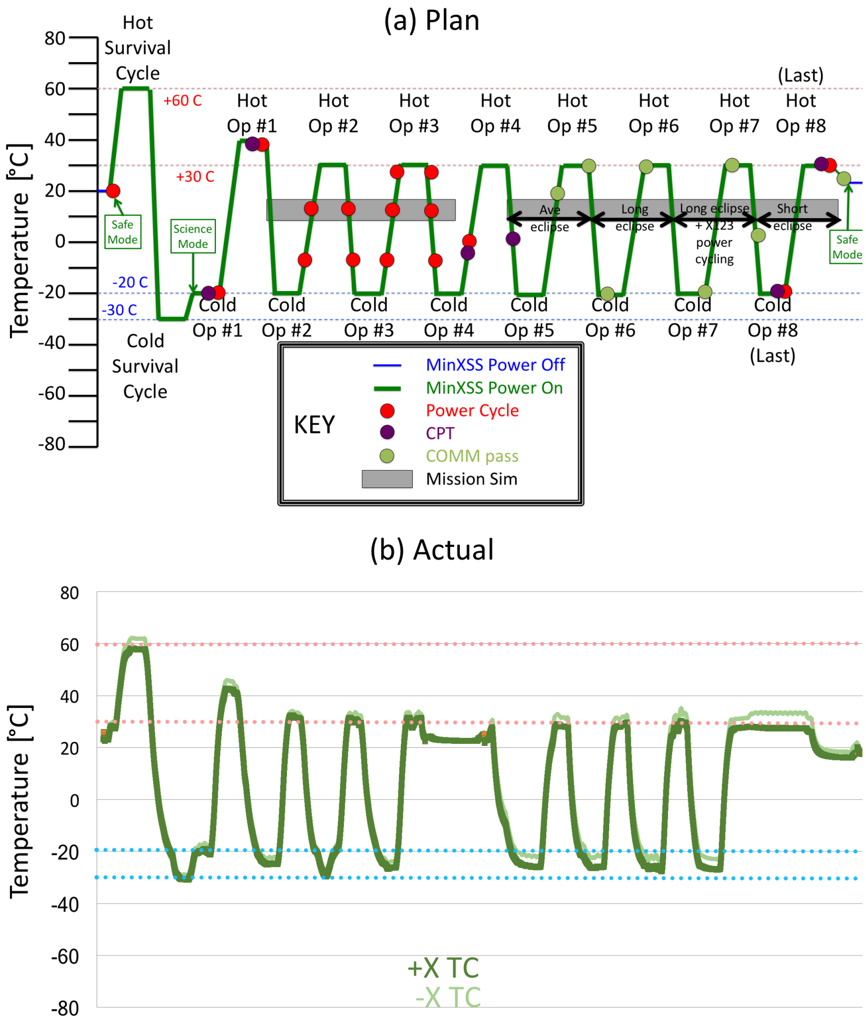

Fig. 4 Thermal vacuum cycle test profile (a) plan and (b) measurements from the X plate thermocouples used for manual control feedback.

B. TBAL Configuration and Procedure

1. TBAL purpose and setup

The purpose of thermal balance (TBAL) testing is to provide measurements for thermal model validation. Additionally, making the chamber resemble an orbital scenario as closely as possible results in a test that is unique from TVAC and boosts confidence in the thermal performance of the spacecraft. To this end, the shroud was made cold to resemble deep space while the platen was made hot to resemble the heat load from the sun (see next section). On orbit, MinXSS actively points one face (+X) toward the sun, so that face was pointed toward the hot platen. Distinctly from TVAC, high conductivity is not desired between the platen and spacecraft. On orbit, the only heat exchange between the environment and the spacecraft is through radiation, so TBAL seeks to emulate this by mounting the CubeSat in the chamber with thick blocks of thermally isolating material (Delrin, in this case), minimizing the surface area contact between the block and the spacecraft, and maximizing the unobstructed view between the platen and spacecraft (Figures 5, 7). In order to validate the thermal model, it is useful to reach a temperature equilibrium point in the test and then to initiate heat load pulses by switching on high-power-consuming electronics (e.g., heaters and the radio) for brief periods of times. This results in heat propagation through the spacecraft that is measured at several points and can be correlated with the model. This aides in determining conductivity across mechanical interfaces for the model.

There were several other differences in setup between TVAC and TBAL. Between the Delrin blocks and the platen, we placed a thin sheet of metal coated with Krylon flat black paint, which has an emissivity greater than 0.95. This improved the radiative coupling between the platen and the spacecraft, bringing it closer to the expectation on orbit while also reducing the time to reach equilibrium temperature. At the start of TBAL, a flight antenna deployment was done to prove the functionality of the release mechanism in vacuum. This meant that the RF hat could not be used.

The radio amplification level was set to 115, corresponding to a measured output of about 0.7 W, rather than its full power setting of 175 (4.7 W output) because the built-in protection on the radio was not at risk of damaging itself at this lower setting. Despite having no "ground-side" antenna inside the chamber, there was still sufficient signal coming through the coaxial feedthrough to use the RF link for communications. Additionally, many more thermocouples were used on the outside of the spacecraft. Where TVAC only had two sensors, one each on the X faces, TBAL had 15 total; Table 3 lists the locations of each, some of which can also be seen in Figure 6.

2. *TBAL procedure*

After the mechanical and electrical interfaces were established, the chamber door was shut and vacuum pulled, while the spacecraft remained off. Once vacuum pressure was obtained, the spacecraft was powered on. No commands were sent to bypass its default startup mode. In this mode, the

Table 3 Thermocouple locations on spacecraft for TBAL. “Top" refers to the +Z direction. As an example, the thermocouples on the -X, -Z, and -Y faces can be seen in Figure 6, identifiable by the strips of Kapton tape.

Face	Approximate location
-Y	Bottom
	Middle
	Top
+Y	Bottom
	Middle
	Top
-X	Bottom
	Middle
	Top
+X	Bottom
	Under solar array
	On solar array
	Top
-Z	Center
+Z	Center

spacecraft believes it has just been ejected so a 30 minute timer counts down to autonomous solar array and antenna deployment. This timeout is a requirement built into CubeSat standards [11**?**]. Through the small viewport into the chamber, 240 frames-per-second video was captured of the antenna deployment. The solar arrays were already in a deployed configuration because deploying them with the abundance of cables present was deemed too risky. The antenna successfully deployed and the spacecraft auto-promoted to safe mode, where it began to beacon every 9 seconds. Just as in TVAC, pressures and temperatures were recorded periodically from this time until the end of the test. The chamber temperatures were then configured – first to the cold thermal balance condition.

In cold balance, the platen temperature was set such that the thermocouple on it (near the

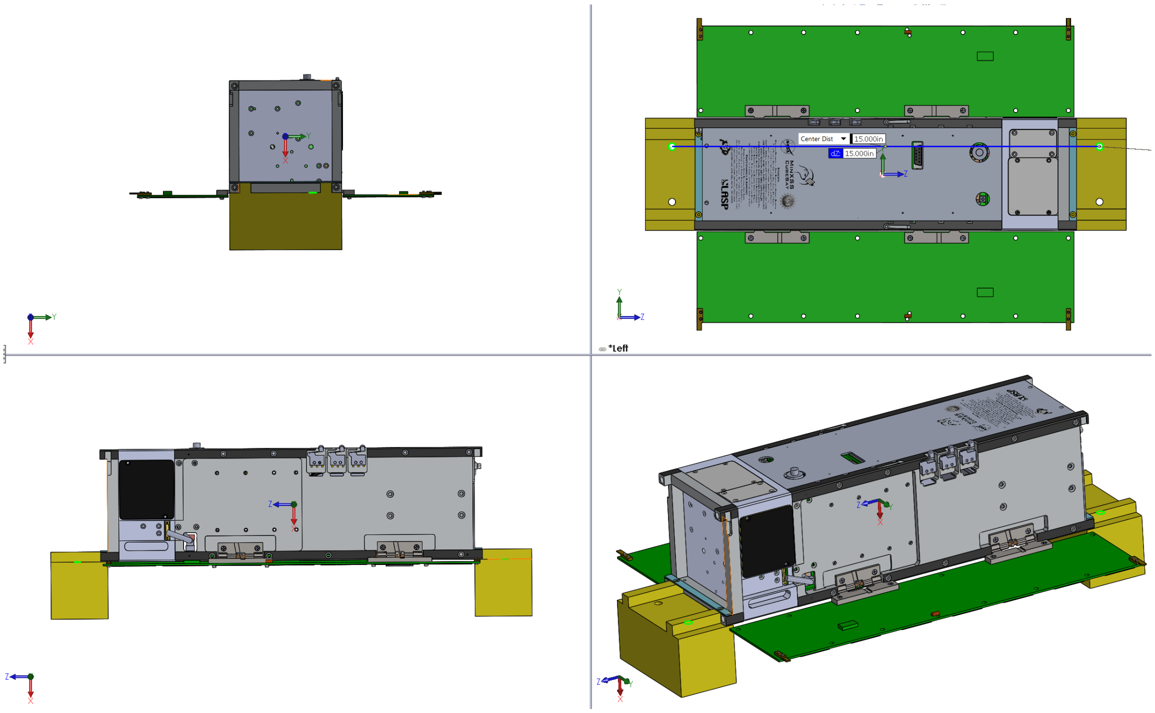

Fig. 5 SolidWorks images of the spacecraft on the custom stand for thermal balance mounting.

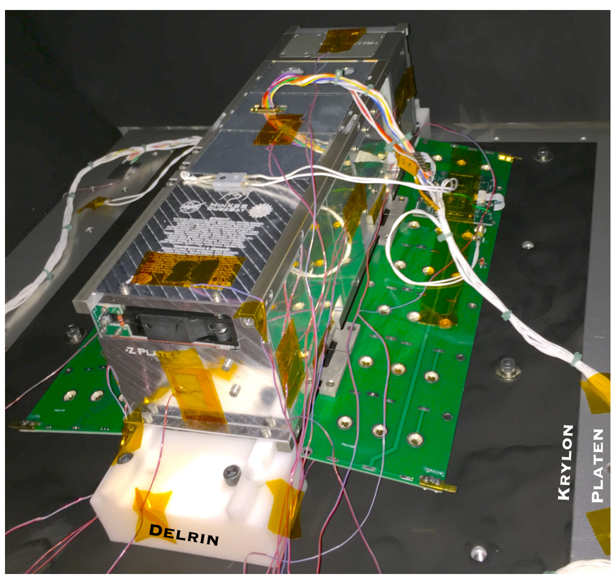

Fig. 6 Picture of the thermal balance setup.

spacecraft) reached roughly +34 °C and the shroud was set so that the shroud thermocouple closest to the spacecraft ("top rear") reached approximately -32 °C (Figure 7). It was discovered that the shroud had a significant temperature gradient ($>$ 30 °C) across its length (Figure 7), which has since been fixed in the chamber. This temperature gradient existed within the field-of-view of the spacecraft and resulted in an overall warmer environment than was targeted. However, the gradient was accounted for in the thermal model configuration (see IV). Additionally in cold balance, orbit simulations of power were performed using the solar array simulator, similarly to TVAC. Only the average eclipse period of 28 minutes was used. This provided a periodic and realistic heat load to the EPS that could then be used for further tuning of the model. Other power cycling was also done. The reaction wheels were generally idle during all thermal testing to minimize the number of stressful cycles placed on them, but they were powered on for three minutes toward the end of an insolated power period in order to determine if there would be an impact to temperatures. The temperature impact was actually observed in the EPS board as more power was flowed through it to the wheels. The CDH board sent beacons for the radio to transmit every 9 seconds but these packets only take ~0.5 seconds to transmit, so the transmitter was unpowered ~95% of the time. Near the end of another insolated power period, the CDH was commanded to transmit sufficient stored data to keep the transmitter on for ~6 minutes, a period of time similar to the reality of on-orbit operations. Radio efficiency, which is a function of power setting, also plays a role in heat dissipation. At the power setting of 105 used in TBAL, the expected heat dissipation in the radio's power amplifier is about 0.6 W; the full power setting of 175 initially used on-orbit should result in a heat dissipation of 10.46 W. However, the intent of this test was to fine-tune the conductivities of the mechanical interfaces between the radio and the Y radiator surfaces, most of which are used for the other daughterboards in the system as well. The difference between the test and orbit radio heat dissipations is not germane to this objective.

In hot balance, the platen TC reached +62 °C and the shroud TC nearest MinXSS reached -11 °C (Figure 7). The SAS output was on for the duration of this test, simulating a fully sunlit period of the orbit. This allowed the system to reach a very stable temperature equilibrium, which provided an excellent baseline for the same power-pulse testing of the reaction wheels and the radio described for cold balance.

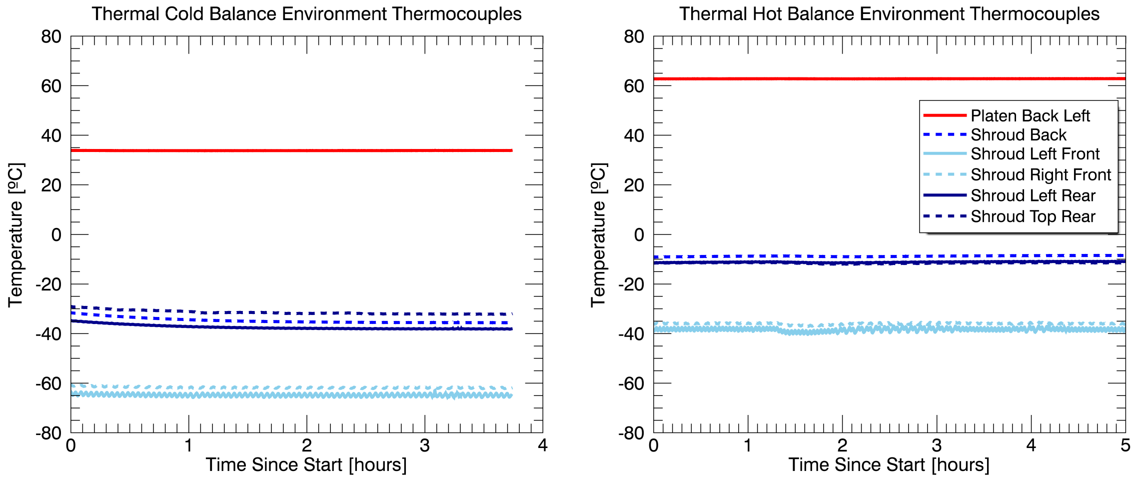

Fig. 7 Temperature measurements from the TCs placed inside the chamber environment during (left) cold and (right) hot balance.

IV. Model

The thermal model was implemented in C & R Tech's Thermal Desktop (TD) version 5.5 – an industry standard thermal analysis tool. This provides the benefit of a graphical user interface with 3D modeling and visualization to the advanced and well-developed thermal modeling in SINDA. The software also has the capability to model orbits.

A. Model Constituents

The TD model for MinXSS consists of 38 physical objects with 319 nodes (points where the model computes temperature), 11 heat loads, 24 contactors (surface-surface conductors), 22 node-node conductors, and 2 heaters (Figure 8, left). The measured mass for MinXSS-1 is 3.52 kg and the model mass is 3.65 kg. Numerous other model checks can be performed in TD, including such sanity checks as “painting" the model with emissivity or other model properties (Figure 8, right).

Physical objects in the MinXSS TD model are represented primarily by rects and bricks. The instrument apertures allow light to enter directly inside the spacecraft and these are modeled as small circles that share their central node with nodes corresponding to the front of the instruments. In this way, light directly impacts the instruments where it would otherwise be shielded by the aluminum

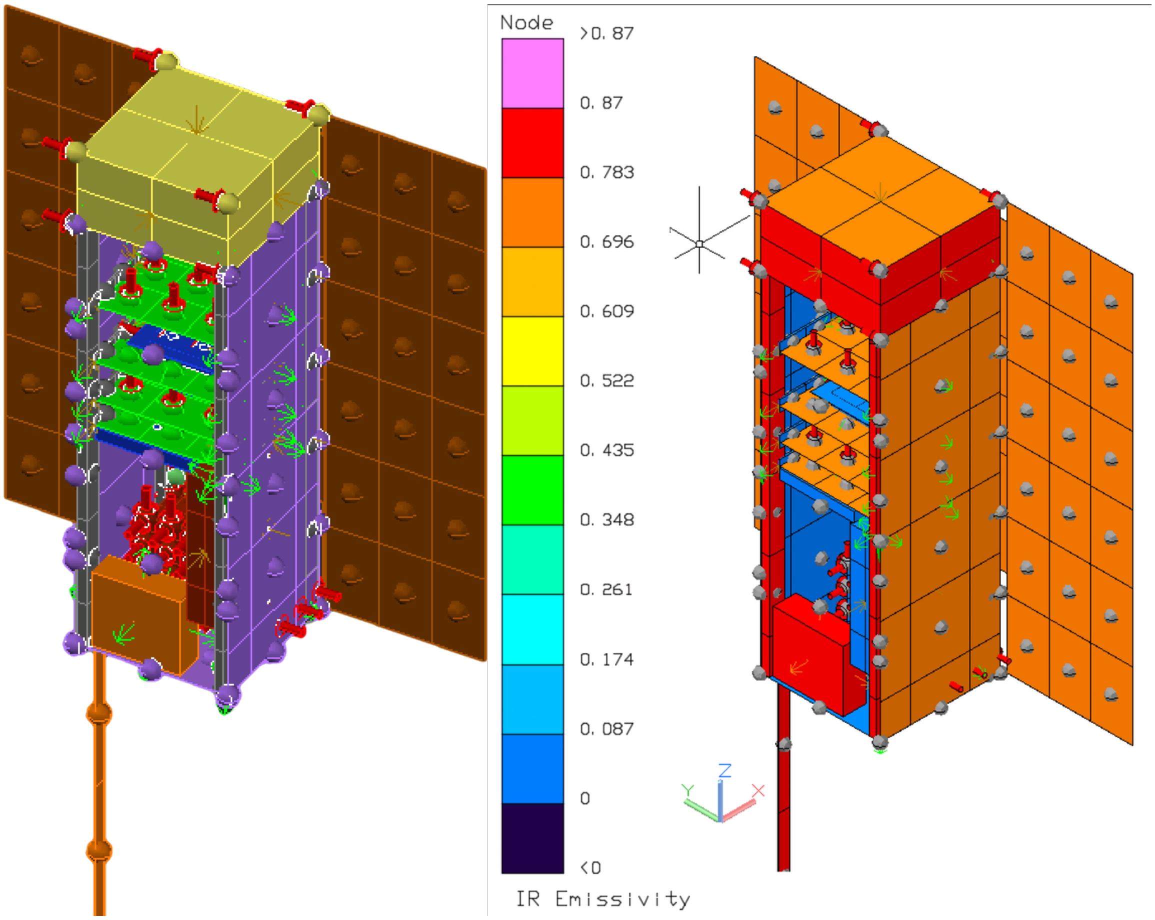

Fig. 8 (Left) Image of the Thermal Desktop model for MinXSS. The colors of the surfaces simply provide contrast for clarity. (Right) Thermal Desktop model check for emissivity. The model surfaces are "painted" by colors corresponding to their infrared emissivity.

structure. TD also allows for many physical properties of rects and bricks to be specified beyond density, specific heat, and conductivity, but these are the only ones necessary for the relatively simple MinXSS CubeSat. Similarly for optical properties, only absorptivity and emissivity were defined for the MinXSS model.

Power dissipation for most components in the model were simple constant heat loads. However, the behavior of the X123 TEC required a more advanced treatment because it draws more power when its heat sink temperature rises. This results in a positive feedback loop because as the X123 draws more power, it dissipates more heat and raises the temperature of the heat sink, which causes the TEC to draw yet more power. Either an equilibrium is reached or the X123 power reaches its maximum and the detector temperature begins to rise. This latter situation has never occurred on MinXSS during testing or flight because the excess heat is sufficiently radiated away. TD can also model heaters, which require the user to specify the wattage and node or surface to apply them to. The power can be constant or proportional to temperature. Two temperatures must be specified: the points at which the heater should power on and off. The MinXSS model only included the two battery heaters because the instrument heater on the inside of the -X face of the spacecraft has been tested with no measured temperature increase observed at other subsystems. This plate simply closes up the spacecraft and its conductive coupling to the rest of the structure is simply too weak to measurably impact the system when the heater attached to it is enabled. Neither is it critical for system operation, so the instrument heater was safely ignored for modeling purposes. Moreover, the instrument heater has never been used in flight.

Many of the user-defined points described above are essentially variables – tunable knobs – for the modeler to adjust in order to achieve correlation of predicted temperatures to measured ones. Most of these have reasonable starting values based on specification sheets, industry standards, calculations, or measurements in the lab. Note that in our testing, we had no way to measure the absorptivity of sunlight, so absorptivity could not be easily or reliably tuned. The appendix provides a listing of all of these variables and their final values. Some values were not modified from their initial estimates while others were tuned to reach correlation between modeled and measured temperatures.

B. Model Environments

1. Vacuum chamber

The critical components of the modeled vacuum chamber for MinXSS were the platen, shroud, Krylon (high-emissivity) plate, and back wall. The platen and shroud have “boundary nodes" that accept user-input constant temperatures, from where heat is propagated across surfaces accordingly. This creates the proper radiative environment for comparison to the measurements. Each element was modeled in 3D with dimensions corresponding to the actual test chamber. The one modification made for MinXSS was the addition of two more boundary nodes on the shroud to account for the measured temperature gradient (Figure 9).

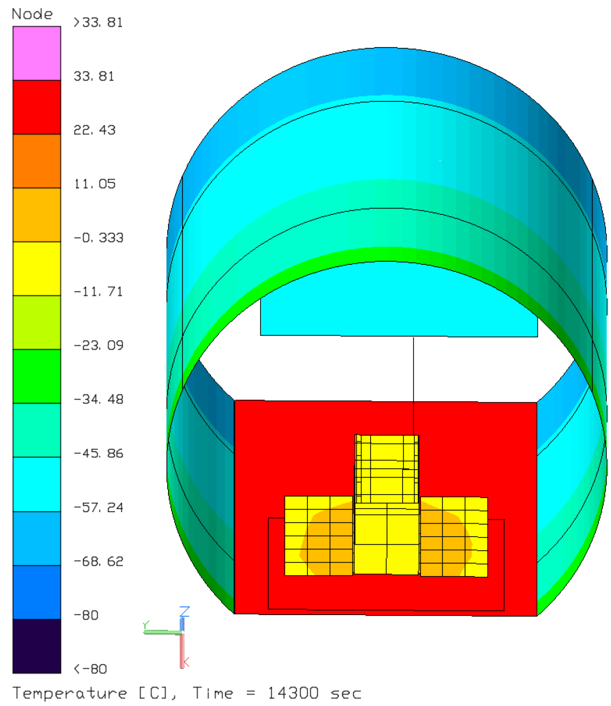

Fig. 9 The MinXSS TD model inside the modeled BEMCO-west vacuum chamber.

2. Orbit scenarios

The majority of CubeSats are deployed from the ISS because of the frequency of launches to that destination and they typically have available space and mass. MinXSS-1 was one such CubeSat. The ISS is at an inclination of 52° at an altitude of 400 km. As such, the orbital precession here results in brief periods of fully sunlit orbits and lengthy eclipses. We define two orbital scenarios for modeling purposes: ISS hot and cold, which correspond to different points in the precession of an ISS-like orbit. The ISS altitude varies over time due to atmospheric drag and periodic boosts to prevent it from deorbiting. In recent years, the ISS has not been above 420 km so this was set as the altitude for the hot case where fully-sunlit orbits are more common and the period of time in sunlight is longer for an arbitrarily chosen orbit. The CubeSat orbit will decay over time and eventually deorbit. The specific altitude of deorbit is dependent on solar conditions and the spacecraft ballistic coefficient, but 350 km is a reasonable low-altitude to consider. At the lower altitude, the solid angle of the Earth is larger and eclipse duration increased slightly. β angle is the primary determinant of eclipse duration. For an ISS-like orbit, β angles above 70° result in fully sunlit orbits and this orbit ranges from β = -75° to +75°. Note that variation in the distance between the Earth and Sun due to Earth's elliptical orbit results in variable input sunlight. This has an impact on the worst case hot and cold cases, but was not accounted for in the final iteration of our model. Table 4 details the orbital parameters used for these scenarios.

Table 4 Orbital scenario parameters.

	ISS Cold	ISS Hot
Altitude [km]	350	420
β [°]	0	75
Sunlight [W m^{-2}]	1361	
Albedo	0.3 below 70° latitude 0.8 above 70° latitude	
Planetshine [°C]	-23.15	

V. Comparison of Predictions and Test Measurements

There are no strict criteria on how well predicted temperatures should match their measured counterparts. Generally, agreement to within 5 °C is desirable and within 3 °C is exceptional. Components with stricter temperature requirements, e.g., the battery's lower limit of 0 °C, should be more closely matched if any predictions indicate they are nearing their temperature limits. Similarly, components with a wide range temperature requirements such as solar arrays or antennas can tolerate a greater discrepancy between model and measurement. This section will first describe bulk temperature comparisons and then numerous comparisons between single temperature measurements and the corresponding model prediction.

First, to get a sense of the bulk agreement between measurement and model, Figure 10 shows all of the sensors internal to MinXSS, thermocouples on the exterior of MinXSS, and the corresponding model values. Rather than plot individual nodes in the model, the TD temperature “measure" tool was used to interpolate temperature near the actual locations of measured temperatures.

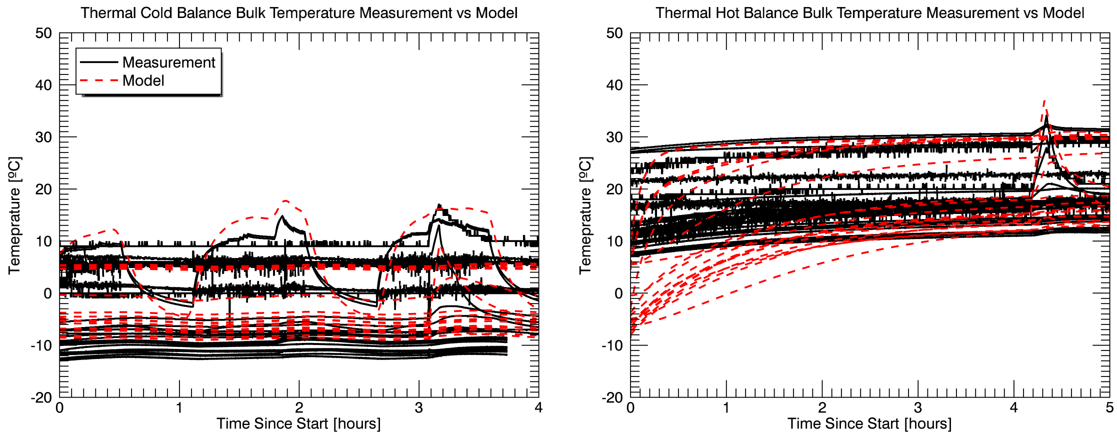

Fig. 10 Bulk temperature comparison between measurements and model predictions for (left) cold balance and (right) hot balance.

In general, Figure 10 shows that the bulk temperatures between measurement and model match to within a few degrees. The cold balance was run with the "steady state before transient" option selected. In a purely transient run, each node starts with an initial temperature of +20 °C, unless overridden by the user. The nodes then begin interacting with the environment via heat transfer and applying heat loads and heater logic. This entire process appears in the plotted data. If run with the steady state prior to transient option selected, the model establishes equilibrium before providing temperatures to be plotted. Variability in this case is due to time-varying heat loads and heaters. For example, the periodic ~hour-long temperature increases are due to the orbit simulation power cycling. The sharp peak around 3.25 hours in the cold balance test is from the 6-minute radio transmission. The peak-on-a-peak feature around 2 hours is due to the reaction wheels being powered on, which manifests as additional power draw through the EPS board.

The hot balance was not run with the steady state option. This allowed us to verify that both options could be successfully used and shows the resulting difference. The hot balance starting point temperatures were overridden with the temperatures at the end of the cold balance run. In other words, the right-most point for each of the red curves in the cold balance plot is the same as the left-most point of the red curves in the hot balance plot. The discontinuity in the measured values (black curves) across the two plots is simply due to the omission of the transition period.

The transition took ~10 hours as the chamber temperatures themselves slowly changed and the spacecraft slowly responded. Plotting this transition would diminish the clarity of the period of interest where correlation is sought. Once at equilibrium, the hot balance case was exceptionally stable because there was no power cycling of the SAS, which is why the black curves are nearly flat until the extended radio transmission at ~4.25 hours. Running the model as a transient shows how the model converges to the environment and that when it does so, it converges to the measured values.

In the cold case, the measured temperatures on the exterior of the spacecraft are systematically colder than the model prediction. These are the black lines below -10 °C. More detailed plots can be seen in Figure 11, showing that the discrepancy is fairly small (< 5 °C). The discrepancy that does exist could be due to the thermocouples not being taped down completely securely, increasing the influence of radiative coupling between the sensors and the environment that was not modeled. Specifically, each thermocouple was covered with a small piece of aluminum tape, all of which was then covered with a slightly larger piece of Kapton tape (some of which are visible in Figure 6).

Figure 11 shows the temperature measurements versus model predictions for the external TCs in both cold and hot cases. All deltas are within the 5 °C desirable limit, with all of the hot balance deltas reaching the exceptional threshold of 3 °C. The power cycling behavior can be seen in the cold balance plots (left column), which provide evidence that the passive cooling system is working. In particular, the SAS provided power via cables plugged directly into the EPS board. The EPS board routes power to all subsystems but is only ~90% efficient, so 10% of that power is converted to heat inside components of the board, primarily in the buck converters that step voltage down from raw, unregulated solar panel voltage to the 8.4 V, 5 V, and 3.3 V levels used in the system. The electrical components conduct heat into the PCB, which contains a copper layer that conducts heat from a localized position to the area of the entire board. At the edge of the board, the Unitrack Kooler-Guide rails have copper-beryllium springs pressing tightly against the edges of the board, where conduction allows heat a path outside the board. The card rails are bolted to the aluminum 6061 Y structure with two #2-56 bolts. There is also direct surface-to-surface contact between the Y walls and the card rails. Thus, conduction allows heat to travel to the Y walls, whose outer surfaces

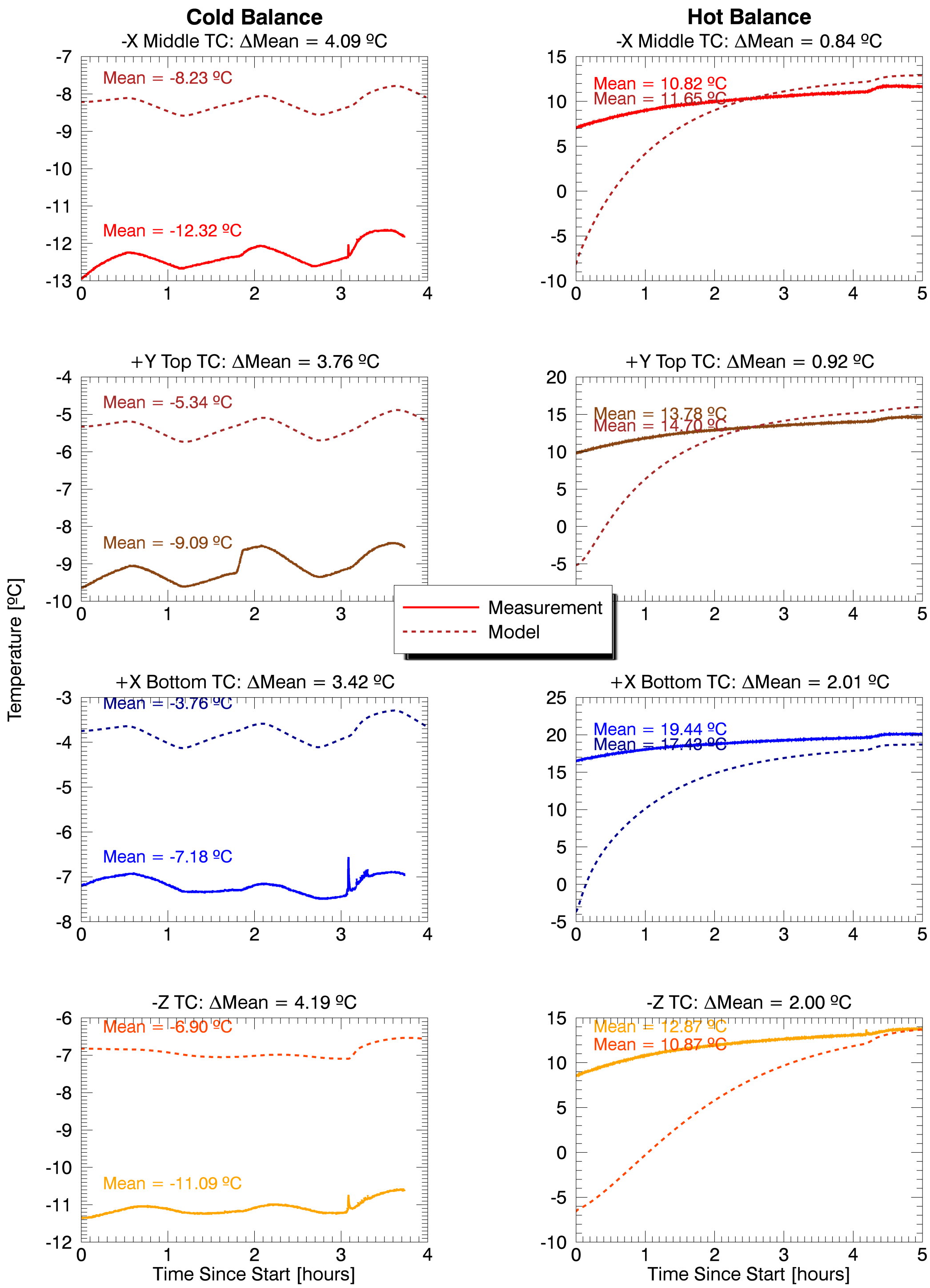

Fig. 11 Temperature comparison between measurements and model for several representative TCs on the exterior of the spacecraft. The left and right columns represent cold and hot balance, respectively. The colors are used simply for differentiation and easier identification.

are covered with silver-coated Teflon tape. This tape has relatively high emissivity (e = 0.84, per the specification sheet) that is the final step in heat release that was generated by the EPS electrical components. Clearly, there are many mechanical interfaces between the buck converters and the radiative surfaces. Each interface results in a small inefficiency in heat transfer because contact between two objects is never as seamless as a single continuous object. Modeling every interface including every electrical component on a board is simply not feasible. Instead, the heat load was modeled as a direct input to the board, with edge contactors defined to the card rails, and the card rails were given face contactors to the Y walls. Each of these have tunable parameters: the heat load can be made to time vary and the amount of power, and the conductors/contactors conductance in W $^{\circ}$C^{-1} can be altered. Forward modeling was used to match the temperature measurements. A reasonable guess was initially input for each of these variables based on calculations measurements, or a specification sheet. For example, the Kooler-Guide rails specification sheet provides a plot of temperature rise versus power, as measured at various positions on the rail with a PCB in it. That information can be used to determine the conductance but is dependent on many factors such as pressure of the copper-beryllium springs (which is itself dependent on PCB thickness), spatial distribution of heat generation, and the temperature of the heat sink for the rail. Rather than try to determine all of this a priori, the model was run and temperatures plotted against those measured. If the prediction showed temperatures on the board were too low, then it can be reasonably assumed the conductivity to the rail needed to be decreased. The model was run again and the predictions compared to the measurements, in an iterative process. For example, this resulted in tuning of the daughterboard to Kooler-Guide rail conductance from 1.07 W $^{\circ}$C^{-1} to 0.02 W $^{\circ}$C^{-1}; the radio to PCB conductance was tuned from 0.5 W $^{\circ}$C^{-1} to 31.62 W $^{\circ}$C^{-1}; and the conductance between the +X solar panel and the +X structural plate was tuned from 0.0346 W $^{\circ}$C^{-1} to 0.2 W $^{\circ}$C^{-1}. Additionally, the power consumption of the system during testing was a known quantity and estimates of subsystem efficiency were made (Figure 12). Here too, forward modeling was applied to achieve agreement between model predictions and measured values.

All of the power coming from the SAS went into the EPS board. The EPS board also has measures of voltage and current in several locations, which can then be compared to the SAS output power to estimate the EPS efficiency. The mean EPS power consumption during this period was

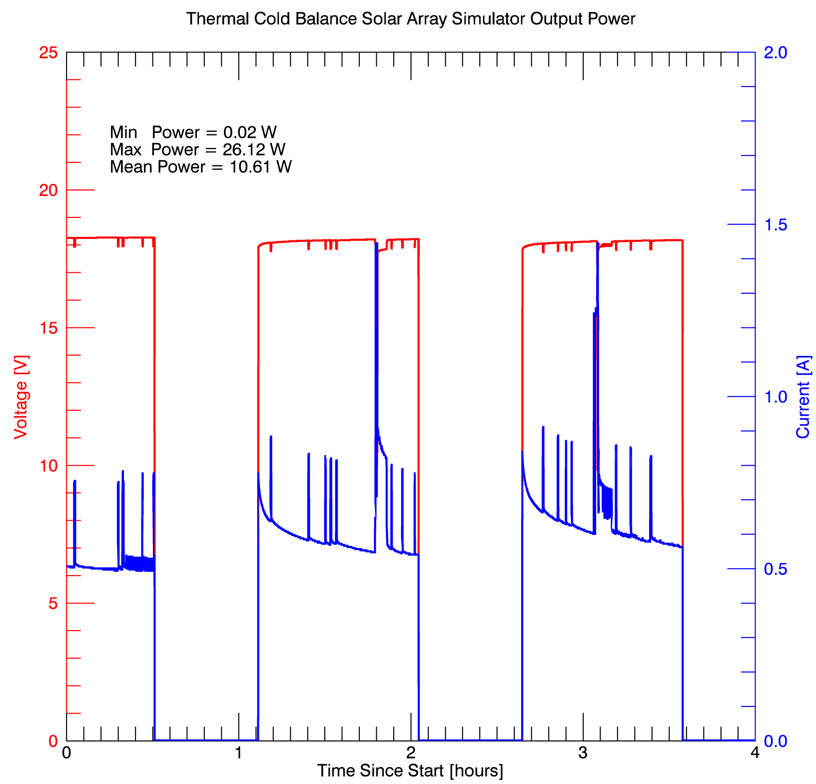

Fig. 12 Output voltage and current from the SAS during cold thermal balance.

9.28 W. Comparing that to the 10.61 W mean from the SAS, the EPS appears to be ~87.5% efficient. Multiplying the 10.61 W input by the EPS inefficiency (12.5%), we obtain 1.32 W dissipated as heat on average in the EPS board. This calculation can instead be performed as a function of time. This was done and used as input into the thermal model by converting the EPS heat load from a constant value to a time varying one with the estimated heat dissipation. Because hot balance had a different power profile than cold balance, the same calculations were done on those data and input in the thermal model to replace the cold balance EPS heat load. The result of these computations is that the modeled temperature profile of the EPS board closely matches the measured values (Figure 13, top left).

Figure 13, focusing on “active" electronics boards, shows that the temperature agreement between the model and the measurements is again quite good. All are within the desired 5 °C, and all but the COMM board in hot balance are within the exceptional 3 °C threshold. The EPS and

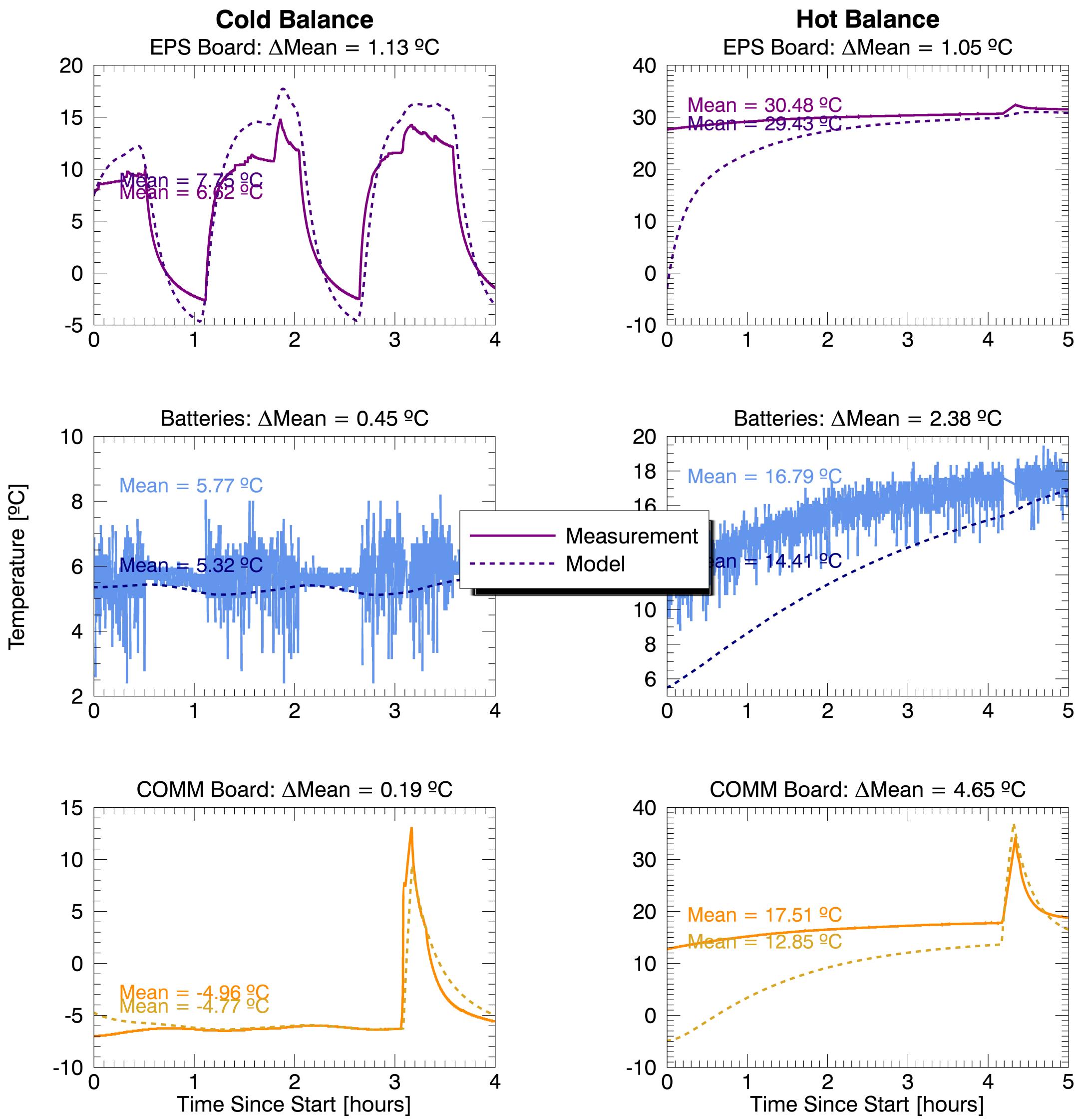

Fig. 13 Temperature comparison between measurements and model for PCBs with time-varying heat loads or heaters. The left and right columns represent cold and hot balance, respectively. The colors are used simply for differentiation and easier identification.

COMM board have time-varying heat loads while the battery board has two heaters. The battery heaters do not trigger in reality or in the model until the battery temperature falls below +5 °C. The measured battery temperature has the additional constraint that at least 2 samples must be below the temperature threshold before flight software will enable the heaters. As can be seen in the measured battery temperature during cold balance, when power is being provided by the solar arrays, the noise on the battery temperature sensor greatly increases. This is due to electromagnetic compatibility (EMC) issues – when there is ~21 W of solar panel power + ~5 W of battery power in the system versus when there is only ~5 W of battery power, we see about 4-5 times the amount of noise on the sensor. Additional EMC filtering (e.g., capacitors) could be inserted into the design to mitigate this but it was not considered a critical issue. The temperature-persistence criteria was never met, so the heaters were never triggered during cold balance. Note that the heaters were triggered during TVAC cold survival and cold operational cycles, which provided assurance that the logic functions properly. As mentioned earlier, agreement between model and measurement should be greater when near critical temperature thresholds. In the cold case for the battery, the measurements and model indicated that the battery was less than a degree above the threshold to trigger the heater. Here, agreement between the two is better than half a degree. The most pertinent temperature for the batteries is their lower-operating limit of 0 °C (see Table 1) but the heater set point is +5 °C to account for thermal "inertia" and uncertainty in the measurement. Also note that there are two battery heaters and two battery temperature sensors in a fully redundant configuration. Only one temperature sensor is shown – the other data are essentially identical.

The model performance for the COMM board (bottom row of Figure 13) is the best of all comparisons in the cold case and the worst in the hot case, but still within the desirable range. The peak around 3 hours is better matched in the hot balance case. These differences are most likely due to heat load modeling versus actual heat dissipation in the radio. Transmission power measurements of the radio were taken (see section VI B) and those data used for the time varying heat load in the model but tuned to achieve good correlation with the thermal balance test results. The radio also consumes power in receive mode, but no measurements were taken of this. Instead, the specification sheet value was used with a small increase to account for the periodic transmitted beacons (approximately 0.5 seconds of transmission every 9 seconds). The large heat pulse generated by the 10-minute transmission was used to fine-tune the conductance values for the Kooler-Guide rails, however. Figure 14 shows the two relevant temperature measurements.

Figure 15 shows the agreement between measurement and model temperatures for the "passive" PCBs in the system. "Passive" in this sense simply means that their heat loads are constant but the boards still respond to heat input via conduction and radiation. Here, all 8 modeled temperature

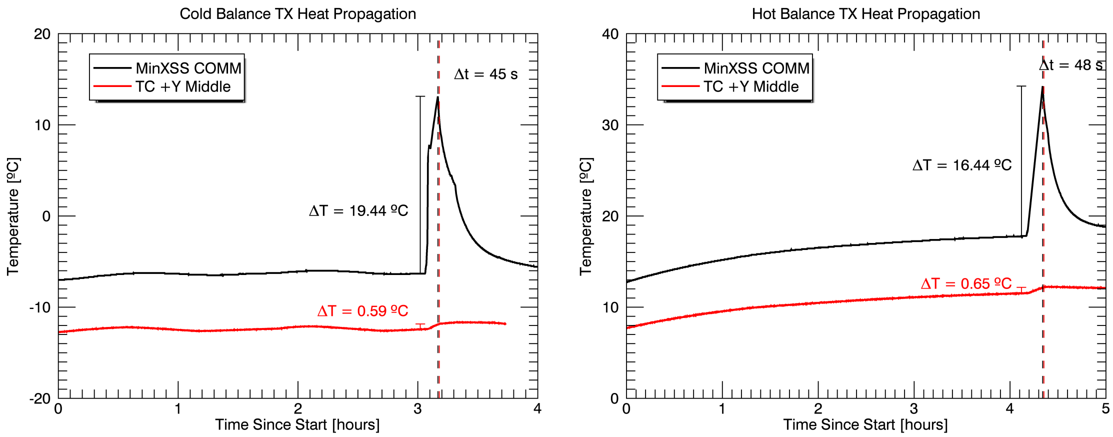

Fig. 14 Heat propagates from the radio to the radiators.

averages are within the “good enough" 10 °C range of the measured values, 7 of which are within the 5 °C desired limit, and 5 of which are within the exceptional limit of 3 °C. The strong temperature response of daughterboards other than the COMM board to the transmission period is primarily due to conduction through the motherboard, rather than through the Y walls. As was seen in Figure 14, the temperature increase in the Y walls was extremely small while the temperature response of the motherboard shown in Figure 15 is much stronger; the ~2 °C increase in motherboard temperature is mirrored in the CDH temperature. This is likely because the daughterboards are connected to the motherboard with 48 pin connectors that have large copper pins soldered to the daughterboard PCB – the conductive path from the copper planes in the daughterboards through the connector is probably stronger than the path through the 8 small copper-beryllium springs in the Kooler-Guide rails. Moreover, the Y plates can directly radiate away any heat flowing into them whereas the heat-loss mechanisms for the motherboard are likely less efficient. Instead, the motherboard acts as a heat-reservoir that all daughterboards (except the battery board) are tapped into.

The body-fixed (+X) solar array has 0.94 mm thick Delrin washers on each of the 6 bolts separating it from the +X structural wall. These were intended to provide some thermal isolation between the array and the rest of the system. Solar arrays on orbit can reach extremely high temperatures – a heat input which is not desired inside the spacecraft where most electronics, especially the X123 TEC, operate better at colder temperatures. The trade-off here is that less

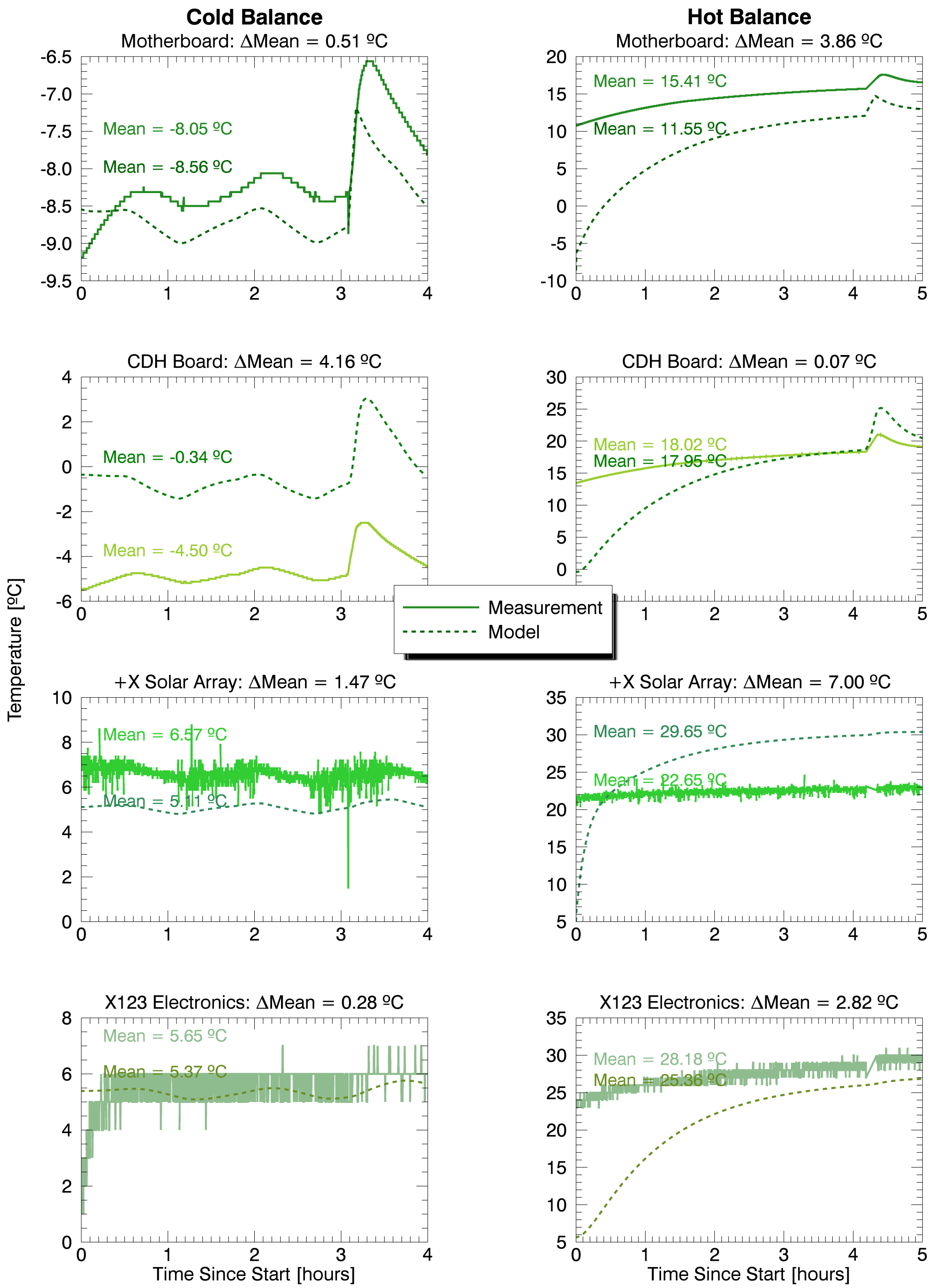

Fig. 15 Temperature comparison between measurements and model for PCBs without time-varying heat loads or heaters. The left and right columns represent cold and hot balance, respectively. The colors are used simply for differentiation and easier identification.

conduction into the spacecraft means the array itself gets hotter and solar cells become less efficient with increasing temperature. There is adequate power margin in the MinXSS system to account for such inefficiencies in the solar cells, however. In order to determine the actual conductance between the solar array and the +X structural wall, TCs were placed on each in the same Y-Z position. If the junction were 100% conductively efficient, the two temperatures should be equal and if it were 0% efficient, there should be a large difference in temperature. Figure 16 shows the measured and modeled temperatures for cold and hot balance in the same format as prior plots.

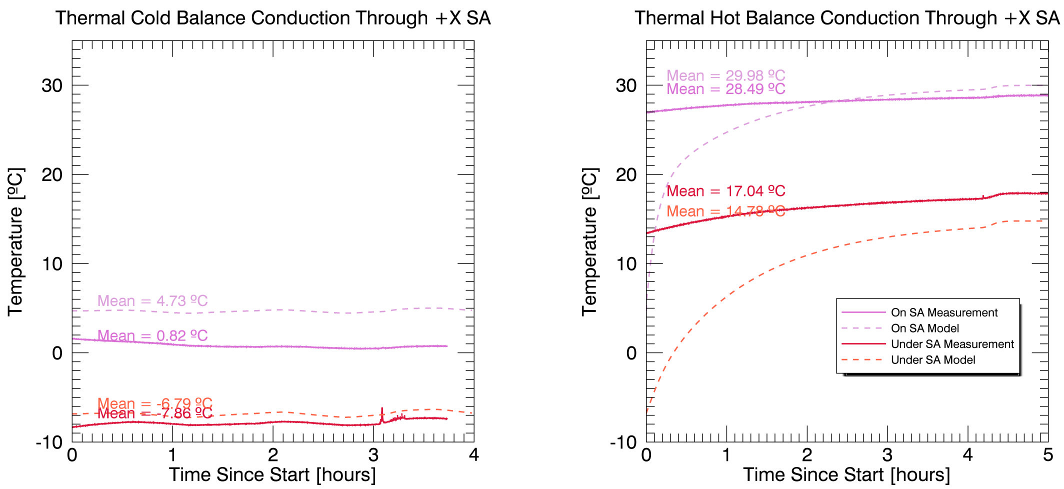

Fig. 16 Temperature comparison between measurements and model for the body-fixed solar array (SA) and the plate it is fixed to. The left and right columns represent cold and hot balance, respectively. The colors are used simply for differentiation and easier identification.

The difference between the measured temperature on the SA and on the structure just below it for the cold case is 8.68 °C on average, compared to 11.79 °C in the model. In the hot case the measured difference is 11.45 °C and the model difference is 15.2°C. Differences like these were used to alter the conductivity between the two surfaces in the model until the above result was obtained. The final conductance was 0.2 W C^{-1}. All such final conductances can be found in the appendix. Figure 17 shows the measured temperatures for the X123 detector, the TC on the nearest radiator surface (-Y bottom), and the total power consumed by the X123. For the cold condition, the mean power was computed across the entire time series. For hot balance, the mean power corresponds to hours 3-4. Note that lab measurements indicated that the X123 electronics box itself accounted for about 0.42 W of the total power. The TEC accounts for the difference between the total power and this constant consumption. The X123 detector temperature value corresponds to the detector itself, which is regulated by the TEC and so does not vary from its set point. What is crucial for modeling is the heat sink side of the TEC and the radiator it is attached to – the -Y plate.

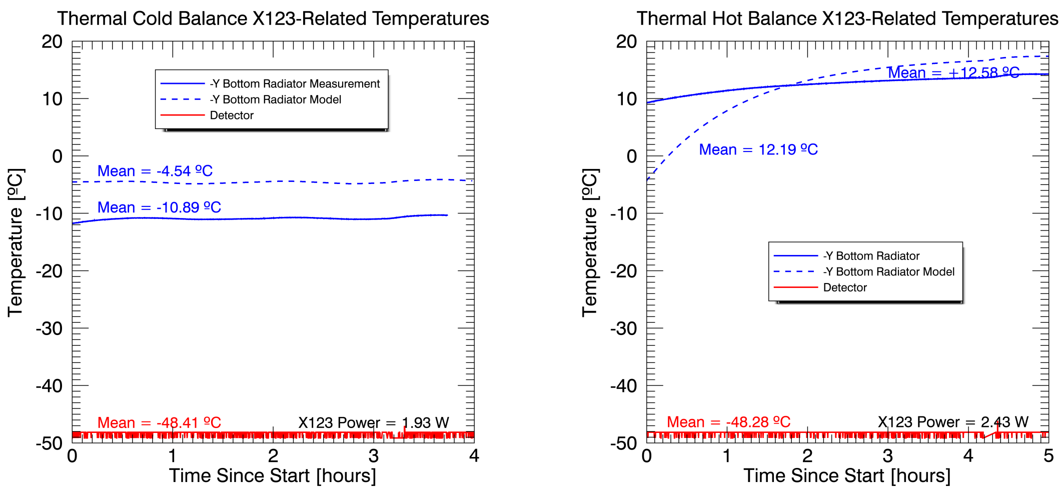

Fig. 17 Temperature comparison between measurements and model for the TC nearest the X123 detector and measurement only for the X123 detector itself. The left and right columns represent cold and hot balance, respectively. The colors are used simply for differentiation and easier identification.

These data were used to create a specialized heat load for the X123 detector in the model. The cold-regulated detector itself is not modeled, instead the TD brick is used to determine the heat sink environment that the X123 detector head exists within. A logic object was created inside TD that accepts temperature input from a bottom -Y plate node and applies a linear relationship (Equation 1) to power based on the power data provided above.

$$tecPower = 0.021 \times heatSinkTemperature + 1.74 \tag{1}$$

where $tecPower$ is measured in W and $heatSinkTemperature$ is measured in °C. The power output from that logic object was used for the heat load of the X123 detector head in the model. In this way, the behavior of the TEC was captured and the positive-feedback loop of the system modeled. This behavior is then easily retained when the MinXSS thermal model is placed in orbit, which is the subject of the next section.

VI. Predicted and Actual Orbital Performance

This section first describes the changes to the model to generate orbit predictions, then compares the model predictions to the measured temperatures on orbit, and finally shows orbital temperature measurements for the entire MinXSS-1 mission to date.

A. Model Changes to Accommodate Orbital Predictions

Two heat loads were altered from thermal balance for orbit predictions: the EPS and radio. In the thermal balance model, measured power data from the cold and hot cases were used to estimate the amount of heat dissipation in the EPS and those time-dependent heat loads were run in the corresponding model. Similarly for the radio, the time-variation in the model was a direct result of measurements from the test. For orbit predictions, the EPS heat load was set to 1.2 W when the spacecraft is in sunlight and 0 when in eclipse. These values were the mean power values from cold thermal balance, which simulated orbital power cycling with the SAS. This method utilized the *hrIllum* parameter automatically generated by TD, which is an eclipse flag. The radio transmit power was increased to the initial on-orbit flight heat dissipation and a realistic periodicity for orbit introduced: every orbit for 5 orbits in a row, the transmission is enabled for 6 minutes. The vacuum chamber structure was also removed from the model.

B. Predicted Temperatures on Orbit And Worst Case Comparisons

Figure 18 shows a summary of how the predicted temperature ranges and actual on-orbit measurements compare to the requirements specified in Table 1. All are within their requirements in both the cold and hot case for the ISS orbit.

The plots in this subsection focus on narrow ranges of time on orbit that have been identified to correspond to the worst cold and hot cases. VI C will show the temperature data over the whole mission to date.

Figure 19 shows several of the predicted external spacecraft temperatures in the same fashion as

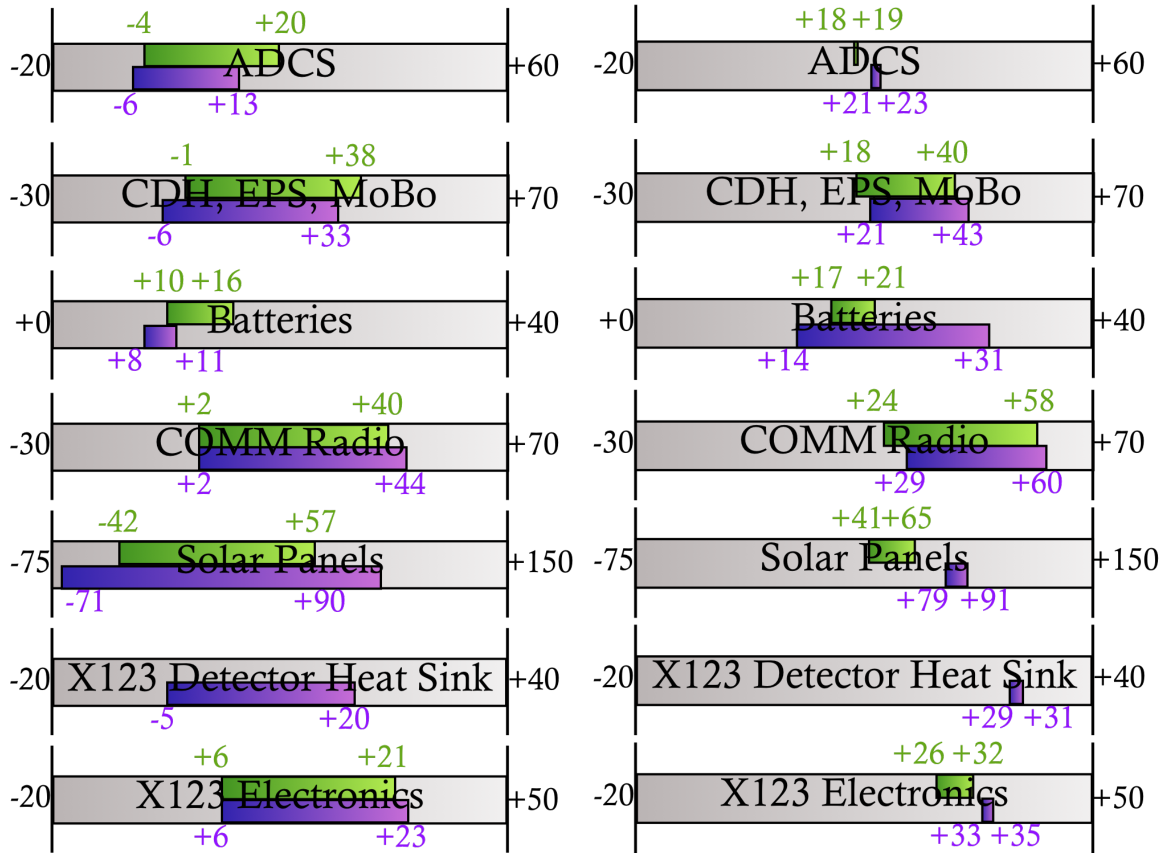

Fig. 18 The maximum range of temperatures predicted (purple) and measured on orbit (green) versus the temperature requirements (grey) for the (left) cold case and (right) hot case.

previous figures. No temperature monitors on the spacecraft surfaces exist in the flight hardware, so a direct comparison to measurements isn't possible here. The increase in temperature from approximately 5-10 hours is due to the radio transmissions during those orbits. It is only clearly visible in the hot case because there the orbit-induced variations are small. It is most clearly identified in the -Z plate because this is where the antenna is bolted and heat readily propagates down the semi-rigid copper cable between the radio and the antenna. Internal testing showed that the X123 TEC can create a temperature difference between the detector and the heat sink of 85 °C. The heat sink is bolted to the -Y radiator plate, and the temperature at the position closest is the -Y bottom (row 2 of Figure 19). With the desired detector temperature of -50 °C, this means the heat sink should be no more than +35 °C. The conduction between the heat sink and the radiator plate is not perfect, however, due to multiple mechanical interfaces. Thus, a radiator plate temperature well below +35 °C is desired. This condition is easily met in the cold case, and is sufficiently met in the hot case. This performance has been verified on-orbit over the 6 month lifetime with the X123 detector temperature measurement (see VI C).

Figure 20 shows the predicted and actual temperatures of boards with strong time variation due to transient heat loads. As expected based on thermal vacuum and thermal balance testing, the EPS board runs 10-15 °C hotter than other daughterboards, such as the CDH. This is a direct consequence of its greater power inefficiency and more power being run through it. Nevertheless, it easily falls between its operating temperature limits of [-30, +70] °C in both cases. The battery temperature plot shows that the heaters will never be needed on orbit when running nominal operations, which has been confirmed. The lowest predicted point in the cold case was about 7.5 °C, while the measurements show it is about +10 °C. The model heat loads are representative of science-mode operations, with all subsystems powered on and regular data downlink periods to the ground. The worst case cold condition would be $\beta = 0$ while the spacecraft is in phoenix mode. In this mode, the ADCS, X123, and SPS are all powered off. In safe mode, the ADCS is powered on and left in its default coarse sun point mode. The intent of phoenix mode is to bring battery charge level up in situations where it has sunk dangerously low and to remove any influence of potential errors with the ADCS. The heaters are only required in this situation, which means that the heaters are sometimes enabled in the most critical power conservation spacecraft state. However, the period of time the heaters are required is inversely proportional to β angle, so this worst case scenario is only representative of a brief period. Additionally, the power draw of the heaters is only ~3 W, compared to the ~5 W of normal load from the other subsystems, and ~10 W of the transmitter. In 12 months of flight, the battery heaters have only been powered on 0.071% of the time. Comprehensive performance tests have established that the time to increase the battery temperature by 2 °C is ~1 minute. The time for them to fall back 2 °C has not been measured, but it is reasonable to assume that the cooling time is of the same order. A ~50% duty-cycle on the heaters results in an average power draw of ~1.5 W. This is a relatively small power draw and only for the very brief period of time corresponding to the worst cold case.

The COMM board temperature is one that must be monitored closely on orbit. It is a strong

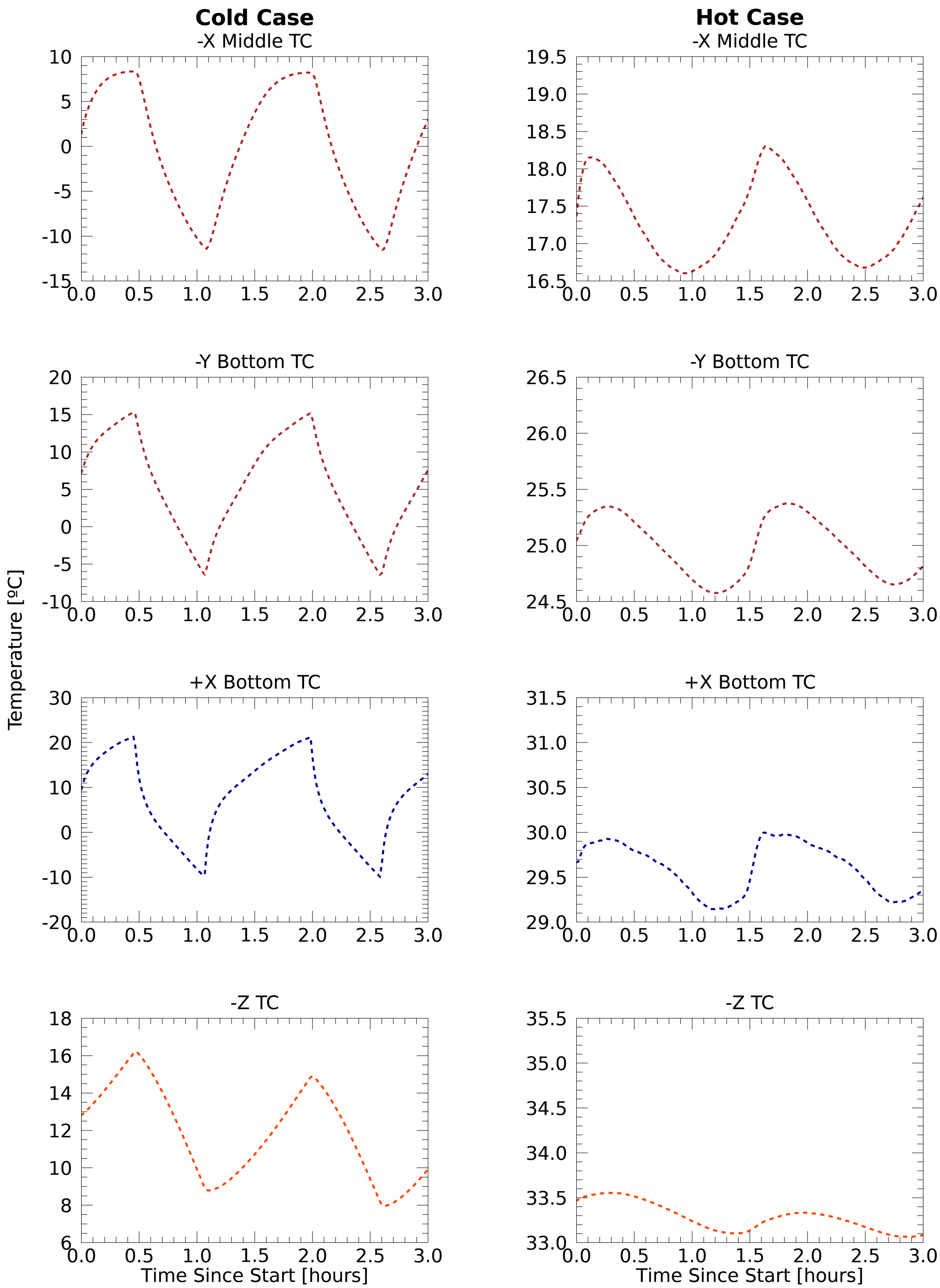

Fig. 19 Temperatures for the predicted cold (left, $\beta = 0^{\circ}$) and hot (right, $\beta = 75^{\circ}$) cases on orbit. The color schemes, plot ordering, and dashed lines have been matched to Figure 11 for easy comparison.

function of the power setting of the radio. Figure 20 is the result of a radio power setting of

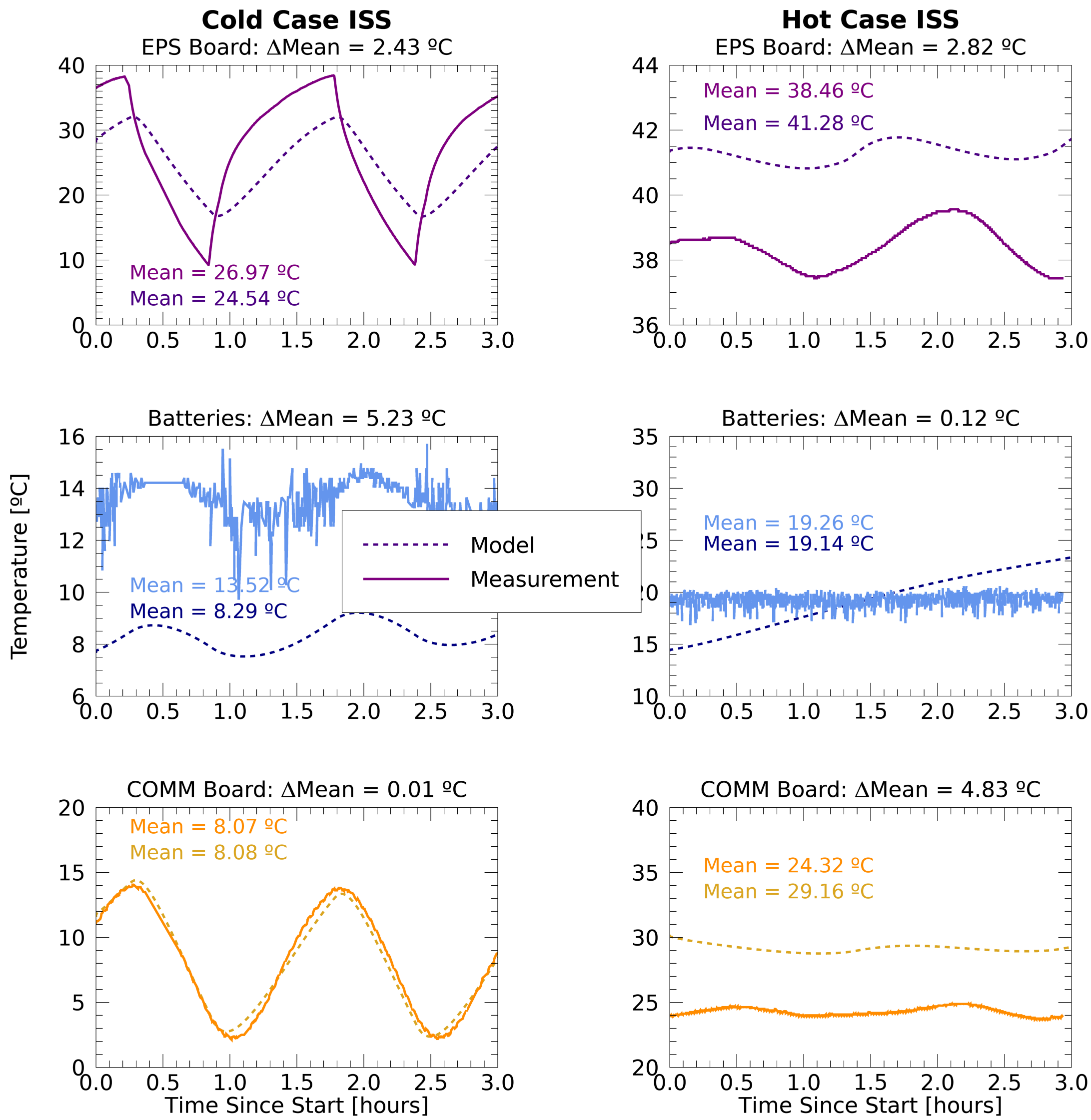

Fig. 20 Comparison of measured and predicted temperatures of the active boards for the cold (left, $\beta = 0°$) and hot (right, $\beta = 75°$) cases on orbit. The color schemes, plot ordering, and dashed lines have been matched to Figure 13 for easy comparison.

140, which corresponds to a calculated heat load of 6.31 W. Table 5 contains measurements of the actual Li-1 radio in MinXSS FM-1. If the model instead uses the maximum power setting and the input power directly, the COMM board temperature reaches 100 °C. Experience with the CSSWE CubeSat, which ran for 2.5 years with the same radio, indicates that the COMM board temperature should be expected to reach about 50 °C. There is uncertainty in that number, however, because CSSWE only had the internal radio temperature on its processor, not an independent temperature sensor closer to the power amplifier of the radio (where most of the heat is dissipated). Indeed, the maximum COMM board temperature observed in the first six months of the MinXSS-1 flight was 56.4 °C, whereas the maximum internal radio temperature was 33.0 °C. Despite these values being within the operating temperature limit of the radio, we have observed issues with the Li-1 radio when operating at these higher temperatures. The primary symptom is un-decodable packets. We reduced the comm amp level on orbit to a setting of 110 (output power of 0.128 W) and still have a stable link without the intermittent decoded packets issue. Note that we recommend that other missions using the Li-1 radio add a heat strap to the radio (we did this for MinXSS-2) and run it at higher amp levels on orbit at least until contact has been established. Reducing the comm amp level can be a part of the commissioning process. Also note that this is not a plan without risk. During internal ground testing, we found that the radio sometimes locks up when the comm amp level command is sent, which causes it to stop transmitting intelligible packets and it begins to rapidly heat. MinXSS flight software was written to mitigate this; the CDH will automatically power cycle the radio if the radio fails to send the CDH its 10-second status packet for more than 5 minutes. This functionality has been verified on the ground but fortunately hasn't been needed on orbit. There is also an additional risk that the radio power level could be reduced to a point where there is insufficient link margin for receipt of spacecraft transmissions. No autonomous software on MinXSS would undo this, but commands could still be used to set the radio power level higher again.

Figure 21 shows the ISS orbit predictions and measurements for the same “passive" PCBs that were shown in Figure 15. Again, the $\beta = 0°$orbit (cold case) with significant periods of eclipse results in wide temperature variation. Note that the estimated β was 1°for the measurements. The motherboard and CDH are well within their operating temperature limits of [-30, +70] °C in both cases. The X123 electronics temperature also falls within the operating temperature limits of [-20, +50] °C in both cases. The solar arrays have the largest temperature variation of any component, as expected. They swing between -20 °C and +80 °C in the cold case and run at a nearly constant 81 °C in the hot case. Here the discrepancy from the model is the greatest, which is almost certainly due to the actual absorptivity being lower than the modeled value. This is because in the thermal

Table 5 MinXSS-1 power measurements with an input voltage of 8.48 V and a 40 dBm attenuator.

Power Setting	Input Current [A]	Input Power [W]	Output Power [dBm] (w/ attenuation)	Output Power [dBm] (w/o attenuation)	Output Power [W]	Efficiency [%]	Heat load [W]
100	0.155	0.57	-33.48	6.52	0.00449	0.8	0.56
110	0.300	1.80	-18.93	21.07	0.128	7.1	1.67
120	0.570	4.09	-11.12	28.88	0.773	18.9	3.31
125	0.770	5.78	-8.22	31.78	1.51	26.1	4.28
130	0.910	6.97	-6.92	33.08	2.03	29.2	4.94
135	0.108	8.37	-5.49	34.51	2.82	33.8	5.54
140	0.121	9.51	-4.94	35.06	3.21	33.7	6.31
145	0.132	10.45	-4.33	35.67	3.69	35.3	6.76
150	0.143	11.38	-4.07	35.93	3.92	34.4	7.46
155	0.152	12.14	-3.75	36.25	4.22	34.7	7.93
160	0.161	12.91	-3.56	36.44	4.41	34.1	8.50
165	0.170	13.63	-3.41	36.59	4.56	33.5	9.07
170	0.179	14.43	-3.33	36.67	4.65	32.2	9.79
175	0.188	15.20	-3.25	36.75	4.73	31.1	10.46

balance test environment it was very dark and there was no solar cell power conversion but on orbit the cells are nominally 30% efficient, which should bring the absorptivity closer to 0.7. The pseudo-peak power tracking system on MinXSS complicates the thermal analysis because excess power will stay on the cells rather than being shunted. Rather than attempt to model this behavior, we simply use the modeled solar cell temperature performance as a bounding worst case. The Delrin washers isolating the +X body-fixed solar array causes them to get hotter, but even the hot case shows that the solar array stays within the operating temperature limits.

Overall, agreement between the model and the measured on-orbit temperatures is good, typically within 5 °C, the major exception being the solar array in the hot case. Fortunately, the actual

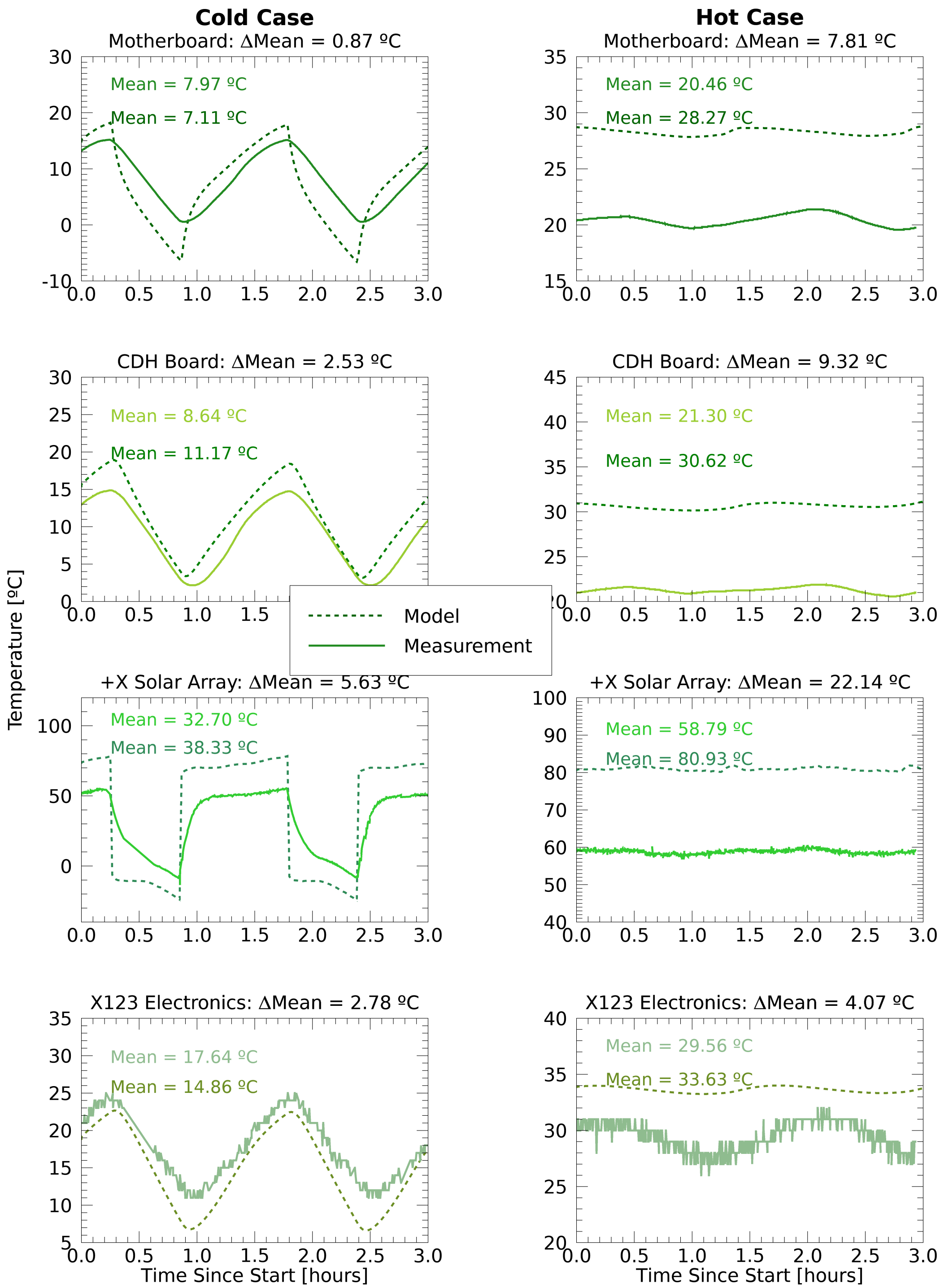

Fig. 21 Comparison of measured and predicted temperatures of the passive boards for the cold (left, $\beta = 0°$) and hot (right, $\beta = 75°$) cases on orbit. The color schemes, plot ordering, and dashed lines have been matched to Fig. 15 for easy comparison.

measurements in that case were further from the operational limits than the predictions indicated, which results in better power performance for the solar cells.

C. Mission-length Temperatures

The plots in this section represent on-orbit temperature measurements over the entire mission to date – about 6.5 months. Figure 22 shows these temperature data with color schemes consistent to the prior figures and dashed lines indicating the temperature limits in Table 1. All components are well within their operating temperatures limits for the entire duration. The one seeming exception is the X123 detector temperature (bottom right plot). The temperature spikes seen here are due to the X123 initial cool down period when powered on. Throughout the mission, we have transitioned to safe mode occasionally for a variety of reasons, which powers off the X123. The detector then drifts toward the spacecraft ambient temperature until it is powered on again and the TEC actively controls the temperature. The X123 detector has a mean temperature of -49.01 °C with a standard deviation of 0.19 °C. The difference from the -50 °C commanded temperature is due to the 1 °C resolution of the temperature sensor. No trend related to β angle appears in the X123 detector temperature, suggesting that the heat sink is sufficiently cold to keep the X123 at its commanded temperature. No temperature sensors directly on the structure exist in flight, so it is only possible to infer this upper bound on its temperature. Nevertheless, the driving requirement has been verified and is consistent with the prediction.

Some of the components have multiple temperature sensors and those are overplotted appropriately in Figure 22. However, the temperatures typically read so close to the same value, it is difficult to distinguish them. The one exception is the temperatures on the body-fixed solar array (+X) versus the deployable solar arrays (Y). Because the deployable arrays can radiate heat to space, they tend to be slightly colder.

It can also be seen that the battery temperature is quite stable despite almost never using the survival heaters. This is a direct result of the thermal design, which thermally insulated the batteries from the rest of the system. From a systems engineering standpoint, we wanted to minimize the use of the heaters because they can have a major impact on the power budget. It was easy to satisfy this with the passive thermal design so such a design was implemented. Nevertheless, we still included survival battery heaters and they were actually triggered on orbit, if rarely. If no survival heaters

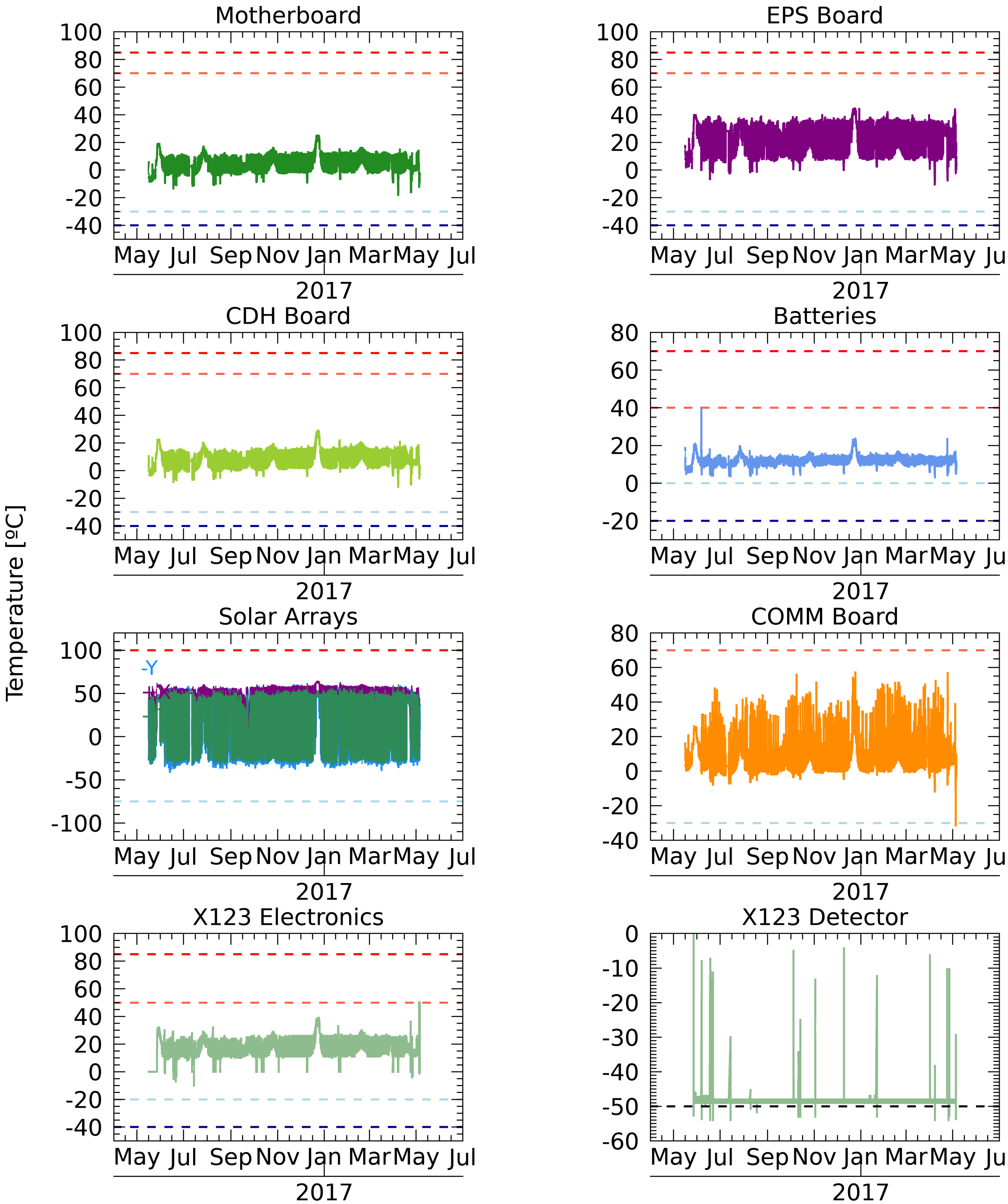

Fig. 22 On-orbit temperature measurements over the life of the MinXSS-1 mission. The dashed lines indicate the operating and survival temperature limits specified in Table 1, except for the X123 detector where it represents the target temperature. The left column correspond to the "passive" components and the right column are the "active" components.

were included, the mission would have been at risk during these periods, and may have ended as early as 3 weeks after deployment (the first time the batteries were triggered). Thus, we strongly encourage all future CubeSats to include survival battery heaters.

VII. Summary and Conclusion

Thermal balance analysis has been performed for a CubeSat in hot and cold environments in order to tune the thermal model for more accurate orbit predictions. All 22 measurement and model temperatures were found to agree within 10 °C. Twenty one of those agreed to better than 5 °C, 14 of which agreed to better than 3 °C. Furthermore, predictions were made for the ISS orbit at high and low β (i.e., short and long eclipse), and all 22 temperatures were within operating temperature limits. Comparison to actual on orbit temperature measurements for the 14 direct points of comparison possible showed that 13 of them were within 10 °C. Nine of those agreed to better than 5 °C, 7 of which agreed to better than 3 °C. The radio is the sole source of concern; its heat load is uncertain and has been monitored closely on orbit to determine if its temperature reaches its upper limit. Although the radio operational temperature limit has not been met to date, temperature-related issues did arise and action was taken to mitigate it: the amplifier level was reduced while ensuring the link remained solid, and MinXSS-2 was modified to include a heat strap for the radio. Now instead of a $>$ 20 °C T as observed on MinXSS-1, we get a $>$ 2 °C T. Thus, it should be possible to run the Li-1 radio at higher amplifier settings as may be necessary given the significantly longer mission length (5 years rather than 3 months). We recommend heat strapping all radios inside CubeSats to avoid these potential issues. Future work could model the effect of the pseudo-peak power tracker on the system. This logic could be modified by other teams for the type of power system implemented on their spacecraft. We also recommend including at least one temperature sensor on the inside wall of the CubeSat as part of the spacecraft telemetry system, but ideally one sensor per radiator surface. This could then be used to more directly determine optical property degradation on orbit [12, 13]. Fortunately, the indirect indication we have on MinXSS-1 from the internal temperatures suggests that there has been little degradation of the silver-Teflon tape in 6.5 months of operation. The average rise in temperature is about 0.3 °C/month. Finally, we find that 1-2 temperature sensors per electronics board is sufficient. In future work, it could be useful to also run the model through periods of temperature transition that actually occurred during the test, using measured chamber control surfaces as model input. Many of the tuned model parameters listed in the Appendices should be applicable to CubeSats that can run thermal models but don't have the resources to do a thermal balance test. The orbit temperatures shown should be representative of a typical case for CubeSats in ISS-like orbits, which accounts for the majority of all deployed CubeSats.

Appendix

Table 6 Thermal Desktop node-node conductors in MinXSS model.

Object A	Object B	Interface	Conductance [W °C^{-1}]	Source
+X structure plate	Y structure plates	4-40 bolts	0.26 per bolt	[14]
-X structure plate	Y structure plates	4-40 bolts	0.26 per bolt	[14]
Antenna	Antenna deployment module	2-56 bolts	0.05 per bolt	Thermal-balance tuned
CDH, COMM, EPS boards	Motherboard	48-pin connector	0.011	Calculated[a]
Radio	Antenna	Semi-rigid cable	0.03	Thermal-balance tuned
Y structure plates	-Z structure plate	4-40 bolts	0.02 per bolt	Thermal-balance tuned
X123 board	X123 electronics box	2-56 bolts and thermal foam	0.038 per bolt	Thermal-balance tuned

$$^{a}\frac{kA}{L} : \frac{(17)(3.414 \times 10^{-7})(48)}{0.0254} = 0.011 \tag{2}$$

Table 7 Thermal Desktop contactors in MinXSS model.

Object A	Object B	Interface	Conductance [W °C^{-1}]	Source
Daughter boards	Kooler-Guide rails	Copper-beryllium springs	0.02	Thermal-balance tuned
Antenna deployment module	-Z structure plate	2-56 bolts	0.105	[14]
Batteries	Battery board	Heat transfer tape	0.03	Thermal-balance tuned
Body-fixed solar panel	+X structure plate	2-56 bolts with Delrin washers	0.2	Thermal-balance tuned
+X structure plate	Motherboard	2-56 bolts	0.05	Thermal-balance tuned
Kooler-Guide rails	Y structure plates	2-56 bolts	0.105	[14]
Radio	COMM board	Solder	31.62	Thermal-balance tuned
SPS/XP	-Z structure plate	2-56 bolts	0.105	[14]
Structure	ADCS	4-40 bolts	0.21	[14]
X123 detector head	-Y structure plate	2-56 bolts and stainless steel bracket	1.07	Thermal-balance tuned
X123 electronics box	-Y structure plate	2-56 bolts	0.105	[14]

Table 8 Thermal Desktop heat loads in MinXSS model.

Name	Applied To	Heat Load [W]
ADCS	ADCS brick	1.94 (orbit[a]) 1.19 (testing)
Battery	Battery brick	0.122 (charging) 0.001-0.016 (discharging)
CDH	CDH rect	0.224
EPS	EPS rect	0 (eclipse), 1.2 (insolated), time varying (testing)
Radio receive	Radio brick	0.09
Radio transmit	Radio brick	0-6.3 (orbit), 0-3.2 (testing)
SPS/XP	SPS/XP brick	0.25
X123 detector head	X123 detector brick	1.5-2.0 (Temperature dependent)
X123 electronics	X123 board rect	0.42
Total		3.68 - 12.50

[b] Some heat loads differ between orbit and testing because the test could not simulate all aspects of on-orbit operation.

Table 9 Thermal Desktop heaters in MinXSS model.

Name	Power [W]	On Temp [°C]	Off Temp [°C]
Battery Heater 1	1.59	5	6
Battery Heater 2	1.59	5	6

Table 10 Thermal Desktop optical properties in MinXSS model.

Name	Applied to	Absorptivity	Emissivity	Source
Aperture passthrough	SPS/XP and X123 apertures	1	0	N/A
Delrin	Antenna deployment module	0.96	0.87	[15]
5mil silver coated Teflon	ADCS +Z, +X plate, ±Y plate, half of -X plate	0.09	0.78	Thermal-balance tuned
Al 6061 bare	Battery encapsulation plates, Kooler-Guide rails, Radio, Structure, SPS/XP, X123	0.031	0.039	[14]
Yellow tape measure	Antenna	0.38	0.8	[15] for absorptivity and Thermal-balance tuned for emissivity
Battery foil	Batteries	0.5	0.04	Thermal-balance tuned
Black anodize	ADCS, structure rails	0.73	0.86	[14]
Circuit board	PCBs	0.6	0.7	[14]
Emcore solar cells	Solar cells	0.9	0.87	[16]

Table 11 Thermal Desktop thermophysical properties in MinXSS model.

Name	Applied To	Conductivity [W in $^{-1}$ C^{-1}]	Specific Heat [J kg^{-1} C^{-1}]	Density [kg in^{-3}]	Source
Aluminum 6061	ADCS, battery encapsulation plates, Kooler-Guide rails, structure, SPS/XP, X123	4.26	963	0.045	[14]
Copper	CDH, COMM, EPS boards	8.6-10.8 (Temperature dependent)	386	0.146	[14]
Delrin	Antenna deployment module	0.009	0.35[a]	0.023	[14]
Lithium polymer batteries	Batteries	0.0051	1011.8	0.035	Best estimate
PCB - FR4	Motherboard, battery board, solar panels	0.01	1[b]	0.03	[14]
Stainless steel 300 series	Antenna	0.40	460	0.13	[14]

[c] These value were used for analysis in this paper but more accurate numbers are in the 2000-3000 J kg^{-1} C^{-1} range for Delrin and 500-1500 J kg^{-1} C^{-1} range for FR-4 boards [14].

Acknowledgments

The authors would like to thank the entire 80+ person MinXSS CubeSat team for their contributions to this successful program. The authors also thank the reviewers for their thoroughness, insight, and dedication. This work was supported by NASA grant NNX14AN84G.

References

[1] Moore, C. S., Woods, T. N., Caspi, A., and Mason, J. P., "The Miniature X-ray Solar Spectrometer (MinXSS) CubeSats: spectrometer characterization techniques, spectrometer capabilities, and solar science objectives," *Proc. SPIE 9905, Space Telescopes and Instrumentation 2016: Ultraviolet to Gamma Ray*, edited by J.-W. A. den Herder, T. Takahashi, and M. Bautz, International Society for Optics and Photonics, Edinburgh, United Kingdom, jul 2016, p. 990509. doi:10.1117/12.2231945.

[2] Woods, T. N., Caspi, A., Chamberlin, P. C., Jones, A., Kohnert, R., Mason, J. P., Moore, C. S., Palo, S., Rouleau, C., Solomon, S. C., Machol, J., and Viereck, R., "New Solar Irradiance Measurements from the Miniature X-Ray Solar Spectrometer Cubesat," *The Astrophysical Journal*, Vol. 835, No. 2, jan 2017, pp. 122. doi:10.3847/1538-4357/835/2/122.

[3] Rodgers, E. M., Bailey, S. M., Warren, H. P., Woods, T. N., and Eparvier, F. G., "Soft X-ray irradiances during solar flares observed by TIMED-SEE," *Journal of Geophysical Research*, Vol. 111, No. A10, 2006, pp. A10S13. doi:10.1029/2005JA011505.

[4] Strickland, D. J., Lean, J. L., Daniell, R. E., Knight, H. K., Woo, W. K., Meier, R. R., Straus, P. R., Woods, T. N., Eparvier, F. G., McMullin, D. R., Christensen, A. B., Morrison, D., and Paxton, L. J., "Constraining and validating the Oct/Nov 2003 X-class EUV flare enhancements with observations of FUV dayglow and E-region electron densities," *Journal of Geophysical Research: Space Physics*, Vol. 112, No. A06313, jun 2007. doi:10.1029/2006JA012074.

[5] Caspi, A., Woods, T. N., and Warren, H. P., "New Observations of the Solar 0.5–5 Kev Soft X-Ray Spectrum," *The Astrophysical Journal*, Vol. 802, No. 1, mar 2015, pp. L2. doi:10.1088/2041-8205/802/1/L2.

[6] Mason, J. P., Woods, T. N., Caspi, A., Chamberlin, P. C., Moore, C., Jones, A., Kohnert, R., Li, X., Palo, S., and Solomon, S. C., "Miniature X-Ray Solar Spectrometer: A Science-Oriented, University 3U CubeSat," *Journal of Spacecraft and Rockets*, Vol. 53, No. 2, mar 2016, pp. 328–339. doi: 10.2514/1.A33351.

[7] Reiss, P., Hager, P., Macdonald, M., and Lücking, C., "New Methodologies for the Thermal Modelling of CubeSats," *AIAA/USU Conference on Small Satellites*, Logan, 2012.

[8] Allison, C., Diaz-Aguado, M., and Jaroux, B., "SatTherm: A Thermal Analysis and Design Tool for Small Spacecraft," *AIAA/USU Conference on Small Satellites*, 2009.

[9] NASA, "General Environmental Verification Standard (GEVS) For GSFC Flight Programs and Projects," Tech. rep., NASA, 2013.

[10] California Polytechnic Institute, "CubeSat Design Specification," 2015.

[11] NanoRacks, "NanoRacks CubeSat Deployer Interface Control Document," 2013.

[12] Gouzman, I., Grossman, E., Murat, M., Noter, Y., Saar, N., Zilberman, G., Minton, T. K., Garton, D. J., Buczala, D., and Brunsvold, A., "A study of atomic oxygen interactions with protected silver surfaces," *Proceedings of the 9th International Symposium on Materials in a Space Environment*, Noordwijk, 2003, pp. 487–492.

[13] Fuqua, P. D., Barrie, J. D., Meshishnek, M., Ciofalo, M., Chu, C.-T., Chaney, J., and Moision, R., "On-Orbit Degradation of Silver Mirrors Exposed to Ultraviolet Radiation," *Optical Interference Coatings*, OSA, Whistler, 2013, p. MD.5. doi:10.1364/OIC.2013.MD.5.

[14] Gilmore, D. G., *Spacecraft Thermal Control Handbook*, Aerospace Press, 2002.

[15] Henninger, J. H., "Solar Absorptance and Thermal Emittance of Some Common Spacecraft Thermal-Control Coatings," Tech. rep., NASA, Washington DC, 1984.

[16] University of Leicester, "University of Leicester CubeSat Project," 2008.